2019

Catalytic Waste Gasification: Water-Gas Shift & Selectivity of Oxidation for Polyethylene

Mason J. Lang
Cleveland State University

CATALYTIC WASTE GASIFICATION: WATER-GAS SHIFT & SELECTIVITY OF OXIDATION FOR POLYETHYLENE

MASON J. LANG

Bachelor of Science in Chemical Engineering

Cleveland State University

May 2017

Submitted in partial fulfillment of requirements for the degree

MASTER OF SCIENCE IN CHEMICAL ENGINEERING

at the

CLEVELAND STATE UNIVERSITY

May 2019

We hereby approve this thesis

For

MASON J. LANG

Candidate for the Master of Science in Chemical Engineering degree

for the Department of

CHEMICAL & BIOMEDICAL ENGINEERING

And

CLEVELAND STATE UNIVERSITY's

College of Graduate Studies by

Jorge E. Gatica

Chemical and Biomedical Engineering Date: _____

Christopher L. Wirth

Chemical and Biomedical Engineering Date: _____

Orhan Talu

Chemical and Biomedical Engineering Date: _____

Defense Date 4/1/2019

CATALYTIC WASTE GASIFICATION: WATER-GAS SHIFT & SELECTIVITY OF OXIDATION FOR POLYETHYLENE

MASON J. LANG

ABSTRACT

As landfills approach capacity and take up valuable land space, metropolitan areas have realized the need for waste disposal alternatives. Thus, there has been a widespread use of waste incinerators in Europe and the United States [1]; [2]. Although newer technology has made incinerators more efficient, there is an increasing interest in formulating 'greener' alternatives to incinerators.

Gasification converts organic and carbonaceous materials into a combination of gaseous products known as "syngas," or synthetic gas. This process greatly reduces the amount of hazardous emissions. The syngas produced by gasifiers has a wide range of uses, including their conversion into diesel, ethanol, methane, methanol and other synthetic fuels [3].

This research consists on an experimental assessment of Low-Temperature Wet Thermal Oxidation (WTO) [4] as a waste management alternative. Detailed experimental assessment and preliminary modeling of gasification technology to process polymeric waste into supply gas is completed here for a model polymer. While catalytic gasification of waste polymers has significance in a variety of engineering applications, it is of particular relevance to in-situ resource utilization (ISRU) and waste management in space exploration beyond low earth orbit (LEO).

The substrates studied in our laboratory, Polyethylene and Cellulose, are both long chain organic polymers, and make up a substantial portion of both space and

municipal waste composition. Although similar in nature, these substrates exhibit marked differences as it pertains to gasification and were therefore selected as model substrates. Experiments performed on polyethylene over a 5 wt% ruthenium catalyst supported by alumina are reported and analyzed in this paper. Analysis of gaseous products using a gas chromatograph with thermal conductivity detection provided data reflecting the conjunctive performance of all reactions. Application of reaction engineering parameter definitions and experimental data enabled the development of a model for the selectivity of reaction products. Kinetic parameters for the oxidation reactions of polyethylene were retrieved. This kinetic information, complemented by the kinetics of the gas-phase reactions (cf. Lange et al., 2018, and Lang et al., 2019), provide the foundation for a phenomenological model for the gasification of solid waste for sustainable living environments.

TABLE OF CONTENTS Page

LIST OF TABLES

LIST OF FIGURES

CHAPTER I

INTRODUCTION

This paper will first cover the analysis of previously published data to retrieve the water-gas shift kinetic parameters. This will complete the gas-phase of the waste gasification kinetic model for catalyst and support of interest. Second, this paper will cover a method of analyzing polyethylene batch gasification selectivity data gathered in the laboratory. This method of analysis will provide a pathway to recovering the reaction kinetics for the carbon dioxide and carbon monoxide oxidation reactions. The recovery of all these reactions' kinetic parameters will mark a significant step in the effort to model wet thermal catalytic waste gasification

One of the most important engineering problems when addressing sustainability and living environments is how to dispose of our persistent waste. Polyethylene, polyethylene terephthalate, nylon, and cellulose are among the major components found in waste. Indeed, polymers make up as much as 40% of approximately 250 million tons of Municipal Solid Waste (MSW) produced by US households [15]. Less than 50% of this MSW was managed by recycling technologies [15]. As landfills reach capacity, it has become imperative to develop and advance alternative methods of waste management. Re-extrusion methods have serious limitations when applied to waste generated in the households (as opposed to industry) and often involve significant costs

[16]. Mechanical recycling methods present an economically viable route, but are limited in application due to the need for single-polymer feedstock [16].

As of 2010 it has been reported that the dry waste stream of space missions consists of 86% packaging waste as polyethylene terephthalate (PET) [6]. All of this polymer waste could potentially be eliminated using gasification, freeing up space for cargo on return trips to earth. At the same meeting, it was estimated that approximately 360 kilograms of methane could be generated every year from the waste of a crew of four [6]. This would provide over 1/3 of the methane requirement for a lunar ascent requiring 4000 kg of fuel at a 3:4 oxygen to methane ratio [17].

Thus reaction-based technologies, such as gasification, present an opportunity to eliminate waste for a wide range of industrial sectors and MSW. More than 80% of the waste generated on the International Space Station is plastic daily packaging waste [6]. A gasification system developed by Santiago and coworkers was able to yield 12-16% CH_4 by weight of plastic used [6].

Other approaches that have been considered are pyrolysis, combustion, and biological methods. The most apparent difficulty presented by pyrolysis and combustion solutions is that they would both likely require temperatures between 350 and 500˚C [18] and between 400 and 1000˚C respectively. Catalytic gasification, by contrast, will require temperatures between 300˚C and 350˚C. Also, pyrolysis may involve a complex product distribution depending on polymer composition; combustion generates carbon monoxide which is toxic. Although carbon monoxide is generated in the catalytic gasification process, it is as an intermediate which can be consumed in the same process to produce the desired methane. Biological methods do not require high temperatures however they

do require environmental controls and only a limited portion of the waste stream may be useful.

The catalytic gasification process begins with the oxidation of a polymer (polyethylene for this example) into CO, CO_2, and water via oxidation. These reactions yield gaseous products that can be further converted into useful fuels such as CH_4 and H_2. The reactions that make this possible are the Water-Gas Shift (WGS) and the Sabatier reactions. The CH_4 and H_2 are potential energy sources while H_2O provides a route to sustain the habitat for crew members and produce O_2 through electrolytic processes; CO_2 can be used as a propellant for small adjustments on space walks.

The most feasible gasification solutions for NASA are required to be simple and energy efficient with little need for sorting and separation of feedstock. WTCO is the gasification process that our laboratory investigates as a candidate for ISRU. The presence of the catalyst reduces reaction activation energies, lowering temperatures and in turn lowering heating costs and improving conversion for exothermic reactions. Without separation of feedstock in the batch reactor, however, the system becomes highly complex. That is to say that the variety of polymer types fed (i.e. polyethylene, polyethylene terephthalate, nylon, cellulose, etc.) means a variety of kinetics for upwards of 10 reactions happening simultaneously.

The move towards hydrogen technology in recent decades has made the water-gas shift reaction particularly interesting to the petroleum industry and to fuel cell technologists alike. Kinetic parameters and models for this reaction have been published and tested over the years for nearly three decades. With these resources available, it is time to apply these numerical values to assessing and designing novel technologies. The

water-gas shift is one of the most important reactions in the gasification process and is essential to building a complete model for catalytic polymer gasification. It is a slightly exothermic reaction ($\Delta H = -41.2\ \mathrm{kJ/mol}$) that favors high conversion at lower temperatures which is how our laboratory runs batch gasification reactions.

Our laboratory has primarily focused on the gasification process over Ru/Al_2O_3 and Pt/Al_2O_3 which are among the materials investigated by Wheeler et al. in their report of kinetic parameters for the water gas shift. They report pre-exponential factors and activation energies for the water gas shift reaction as well as selectivity data for methanation which can be explained by the Sabatier reaction.

Methanation has been reported to occur at the greatest degrees in experiments on Ru-based catalysts. Due to this, one must reconcile the presence of the Sabatier reaction with the kinetic parameters retrieved for the water gas shift. Moreover, in order to use the kinetic parameters retrieved by other authors it is imperative that we reconcile their assumptions with the conditions of our experiments; so that the results may be used in conjunction with the data which characterizes gasification of long-chain polymers typically found in municipal or space exploration waste.

With both the Water-Gas shift and the Sabatier kinetic parameters known for catalysts of interest (cf. Lange et al., 2018, and Lang et al., 2019), what is left is the need for kinetic parameters to describe the liquid-phase oxidation reactions (Equations 1 & 2). In an optimal gasification process, as much substrate (in this case polyethylene) would react to form CO (as opposed to CO_2).

Retrieving data for the conversion of the substrate in a full gasification process is possible. However, isolating these results from the effects of the gas-phase reactions to

perform an analysis that yields the independent kinetic parameters of each of the two oxidation reactions requires some manipulation of the data. A method of analysis has been devised wherein the selectivity of each of the detectable components (using gas chromatography) can be differentiated with respect to residence time to obtain information on the rates of each of the two oxidation reactions. Any information that can elucidate the competition between these two reactions is highly desirable for purposes of optimization. Unfortunately, unlike the gas-phase reactions, experimental data needed for these results must be collected on a substrate-by-substrate basis. Thus, in this thesis, the discussion will be limited to the selectivity of oxidation for polyethylene. However, once the kinetic parameters for polyethylene on a ruthenium catalysts are known, the entire kinetic model for the wet thermal catalytic gasification process for polyethylene will be completely numerically described. This will be a major step towards an applicable understanding of the highly involved waste gasification concept.

The wide range of applications and the advancement of technology for plastic solid waste have had the double-sided effect of providing inexpensive material solutions to innumerable industries while contributing to a daunting solid waste problem for the world. Al-Salem et al. determine in their review that chemical recovery methods for waste polymer recycling demonstrate potential for robust application and are worthy of investigation as solutions to municipal solid waste. According to Al-Salem et al., mechanical recycling presents clear disadvantages: limiting criteria for feedstock, intense energy consumption, and limitations on byproducts [5]. They further claim that chemical methods appear more promising than mechanical recycling methods. Gasification is one of a few technologies that falls under the chemical category for recycling plastic solid

waste. “Although large industrial scale units do exist for both pyrolysis and gasification, a fact remains that most of them could perform more effectively targeting certain products depending on feedstock, market performance and demand. All of such issues could be solved by end-product unit design [5]” Results in kinetic analysis of gasification will make this design possible.

Another more focused application of waste polymer gasification is In-Situ Resource Utilization (ISRU) which is an initiative by NASA to find methods for converting onboard materials into valuable products. Santiago et al. highlight the need for a solution to the problem of waste accumulation on the International Space Station (ISS) and space expeditions in general [6]. They provide elemental weights for the waste stream of a four person crew and design a full process laboratory scale gasification system. They perform tests on polyethylene and report yields of 12-16% methane by weight of plastic used. The importance of methane as a product becomes apparent in the context of space exploration due to the fact that Mars’s atmosphere already contains high quantities of carbon dioxide. NASA seeks options for generating fuel on Mars in order to reduce the required mass of propellant at the “Earth departure stage” and make long-duration space missions to Mars possible. Designing processes that produce maximum quantities of hydrogen does not utilize the advantages for fuel production offered by Mars’s atmosphere. Thus, both the water-gas shift reaction and the Sabatier reaction are both equally important reactions in the research of catalytic waste gasification.

Working with the water-gas shift reaction, the Sabatier reaction provides the means for methane production in catalytic waste gasification. The experiments performed by Lunde and Kester provide data from which the kinetic parameters for the Sabatier

reaction could be calculated [7]. These values would be necessary for use alongside the water-gas shift kinetic parameters to develop a comprehensive model for the catalytic gasification of waste polymers.

In order to retrieve the kinetic parameters for the Sabatier reaction, Lange et al. looked to the experiments of Lunde and Kester. Discovering that the model used by Lunde and Kester only considered the outlet partial pressures for rate law, Lange et al. examined a model that considered the average partial pressure for each species throughout the packed bed reactor. Lange demonstrates the superiority of the average pressure model for plug flow and packed bed reactor kinetic expressions but also highlights some of the potential weak points of the analysis and highlights certain assumptions for future verification [8]. We can also retrieve the parameters for the water-gas shift reaction from other laboratories' experimental data. In order to increase its robustness, Lange et al. investigates the assumptions of the Average Pressure model originally proposed and exercises several verifications testing these assumptions. One of these is the comparison between the outlet partial pressures recorded in the experiments of Lunde and Kester and those calculated using the Average Pressure model. Another point of verification was the comparison between the outlet partial pressures calculated using a linear average and a non-linear average of the reaction rate throughout the packed bed reactor.

The effort to determine the nature of the water-gas shift reaction under a wide variety of conditions has been an ongoing search for at least three decades. With the wide range of operating conditions and catalyst properties being applied to water-gas shift experiments around the globe, it is difficult for designers to find kinetic parameters and

expressions that will accurately predict the reaction rate for their particular systems. Smith et al. have extensively reviewed the numerous studies in catalytic water-gas shift kinetics and organized the results of these studies based on catalyst type, approach to the kinetic expression, as well as the differences in suggested reaction mechanisms and intermediate structures within those kinetic models. Smith et al. notice that the approaches to the kinetic expressions for the water-gas shift are either microkinetic or macrokinetic (empirical). The article concludes that most of the articles reviewed conform to power law kinetics and hence this may be a safe assumption in the development of further water-gas shift models. Smith et al. also note that Pt may show the most promise among the noble metal catalysts for commercial use [9].

Looking more closely at the impact of catalyst on the water-gas shift reaction, Grenoble et al. conclude that ruthenium is a more effective catalyst than platinum [10]. With the likelihood of application seen in platinum by Smith et al. and the particular effectiveness of ruthenium for not only the Sabatier reaction, but the water-gas shift as well, a closer look at the performance of these noble metals could provide better insight to the real potential of waste gasification.

Contributing to the research into precious metal catalysts for the water-gas shift reaction and the supports being developed for them, Utaka et al. prepare their own catalysts for experiments with water-gas shift. The article proposes a need for research into the effectiveness of precious metal catalysts beyond copper due to the fact that, despite their popularity, copper-based catalysts are highly vulnerable to deactivation in oxygenated, hydrated environments. Considering the fact that the data collected in our own experiments reflects gasification capabilities at low temperatures using ruthenium

and platinum catalysts supported by alumina, the data collected by Utaka et al. is particularly useful. They investigate ruthenium and alumina extensively: “Though ruthenium and rhodium catalysts had similar catalytic characters with high activities, the ruthenium catalyst had high activity at lower temperature, 250 °C. The CO conversion of the Ru/Al_2O_3 was the highest, while it was active for the methanation reaction. However, we consider that high activity of the Ru catalyst will become attractive for the shift reaction if methanation is inhibited [11].” They finally conclude that the activities for the reaction depended more heavily upon the chemical character of the oxide supports rather than the surface area or dispersion of ruthenium. They highlight the superiority of a Ru/V_2O_3 catalyst over all others investigated.

Answering questions raised by the conclusions of Utaka et al., Panagiotopoulou & Kondarides look more closely at the nature of the supports of water-gas shift catalysts. They discover that Pt and Ru catalysts for the water-gas shift reaction are much more active on “reducible” rather than “irreducible” metal oxides (ex. Ti_2O_3 vs. Al_2O_3) [12].

The work of Wheeler et al. provides kinetic parameters for both ruthenium and platinum catalysts. Their experiments involve water-gas shift reactions in a packed bed reactor at contact times ranging from approximately 10 to 18 ms and temperatures between 300 and 1000 ˚C. Water was fed in excess for the reactions and hydrogen was also fed. The model developed by Wheeler et al. assumes that water and hydrogen remain constant throughout the reactor and thus their concentrations (or partial pressures) are excluded from the rate equation. In addition to this empirical model, the article also includes a microkinetic description of the water-gas shift with a Langmuir-Hinshelwood kinetics model following the sequence of a noble metal mechanism.. The article provides

a table of pre-exponential factors and activation energies with which the rate of the water-gas-shift may be predicted for different catalysts [13].

Choi et al. investigate the effect of several factors, primarily steam/carbon ratios and reactor temperature, on the conversion of CO in a micro reactor testing unit on copper catalysts. Their findings indicate that higher steam/carbon feed ratios results in higher conversions of CO. They propose that both the regenerative and the adsorptive microkinetic models describe the reaction equally well and apply an empirical rate expression described using power law kinetics and two parameters to fit the data nearly as well as the microkinetic models [14]. They calculate activation energies in the rage of 40 to 70 kJ/mol for copper with variation in supports such as alumina and zinc oxide. MATLAB was used to minimize a sum of squared residuals by finding the parameters for the nonlinear functions. The regenerative mechanism expressed in Langmuir-Hinshelwood kinetics was the best fit for the data although no model performed with R below 0.986 [14].

CHAPTER II

THEORY

This chapter will cover several topics as they relate to retrieving the kinetics for the reactions of waste gasification. Knowing that the kinetics of the gas-phase reactions remain unchanged regardless of feedstock composition, the first task of this thesis was to recover the kinetics for the water-gas shift (WGS) reaction. This was done using another laboratory's data and proposing an improvement in the model for the reaction. Next, selectivity data from *our* laboratory is used to recover ratios of the liquid-phase oxidation kinetics for polyethylene gasification over a ruthenium-on-alumina catalyst.

Kinetics of the Water-Gas Shift Reaction

As described in the introduction chapter, the water-gas shift (WGS) reaction is essential to the waste utilization process as a means of producing hydrogen (see Equations 1 & 2) Hydrogen not only serves as a valuable product in its own right, but allows for the transformation of carbon dioxide via the Sabatier reaction into methane; which is highly valuable due to its potential to fuel energy recovery.

These two reactions make up the gas-phase part of the gasification process. Previous research in the group yielded the Sabatier kinetics [8]. A kinetic model for the

gasification process requires knowledge of the kinetic parameters for *both* gas-phase reactions.

Because the gas-phase reactions remain the same regardless of the feedstock or polymer type in the gasification process, the parameters for the WGS and the Sabatier reaction once found can be applied to waste gasification technologies regardless of the substrate gasified. This lack of necessity for a specified feedstock means that the kinetics for these reactions can be retrieved from other laboratory's experimental data. Although the papers containing this data normally also contain their own analysis with reported parameters, it is often required to adapt the original analysis to the conditions in the process investigated in this Thesis.

Since the water-gas-shift reaction is common to several technologies, there are several studies in the literature providing data as well as reporting the kinetic parameters for a wide range of conditions and catalyst. Indeed, one of such references corresponds to the study of Wheeler et al. [13]. Figure 1 illustrates data for the WGS collected for a variety of catalytic and support materials.

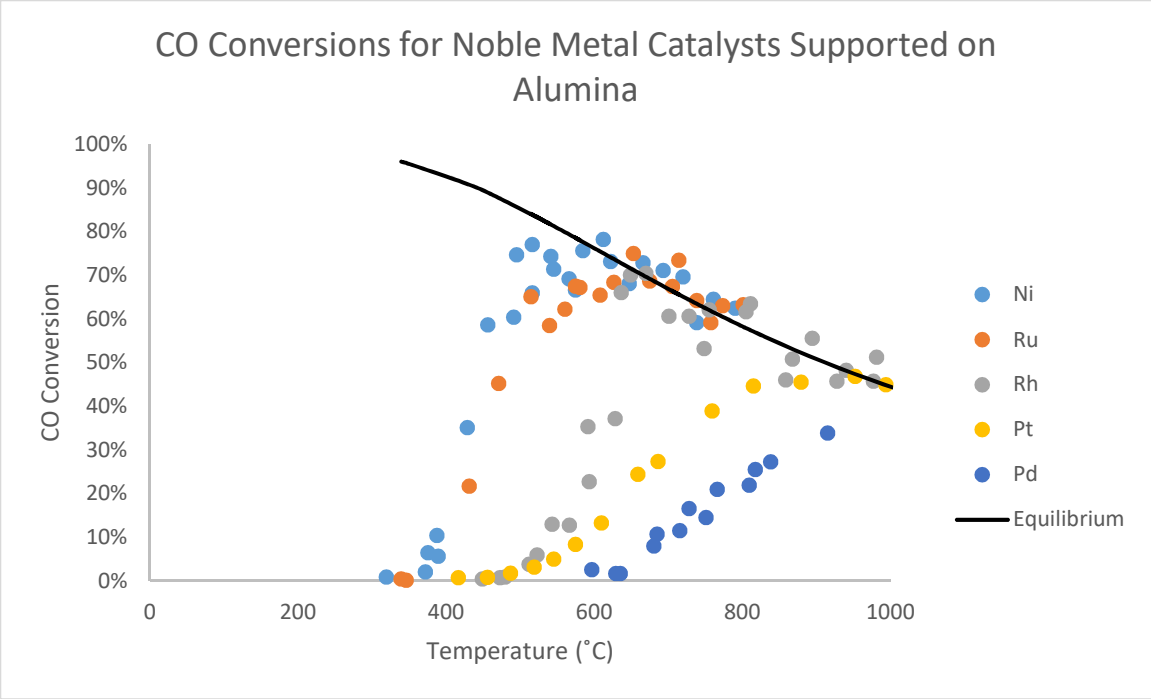

Figure 1: Carbon Monoxide conversion data for noble metal catalysts supported at 5 wt% on Al_2O_3 support foam monolith. Feed conditions: CO, 11.4%; H2O, 45.7%; CO2, 0%; H2, 22.9%; N2, 20% at 1 atm and 3 SLPM. Support monolith had diameter of 17 mm and length of 10 mm. Void fraction was 0.8. Plot is adapted from Wheeler et al. [13]

A model is proposed with the kinetics in the report. Initially, the model for the reaction is proposed to be power-law first order with respect to all species [13]

$$-r_{CO}^{w} = k_f^{w} P_{CO} P_{H_2O} - k_b^{w} P_{CO_2} P_{H_2} \quad (1)$$

This rate equation suggests that the rate of consumption of carbon monoxide is subject to the changes of every component involved in the water-gas shift reaction. This approach to modelling the WGS has been taken by several other labs [10] [19] [20] [21] [22]. However, the author makes an assumption to simplify Equation 1 [13]. This assumption may be inappropriate for the application of interest. In order to understand the assumption more clearly, the data can be extracted to derive the same model from the beginning. An

alternative model will be proposed when the assumption proves unsatisfactory for our application.

Selectivity of Methane

Before the data can be used, however, the presence of the Sabatier reaction must be taken into account. Indeed, high degrees of methanation were reported for the ruthenium-based catalysts (see Figure 2).

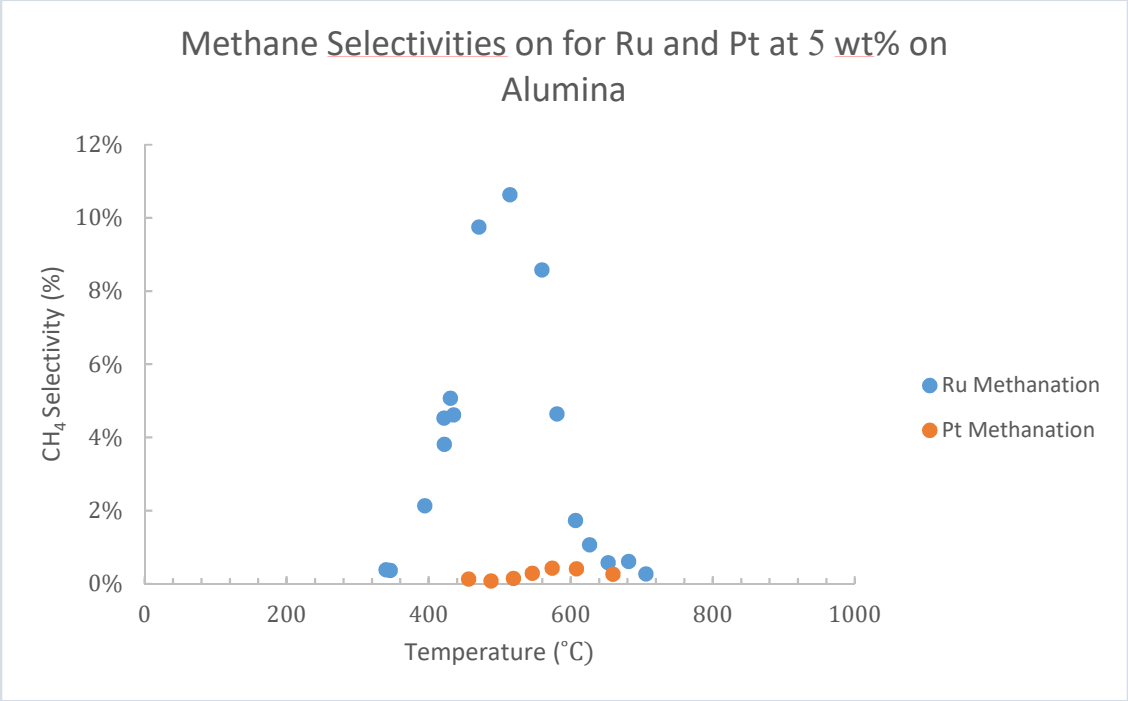

Figure 2: Methane Selectivity data for noble metal catalysts supported at 5 wt% on Al2O3 support foam monolith. Feed conditions: CO, 11.4%; H2O, 45.7%; CO2, 0%; H2, 22.9%; N2, 20% at 1 atm and 3 SLPM. Support monolith had diameter of 17 mm and length of 10 mm. Void fraction was 0.8. Plot is adapted from Wheeler et al. [13]

The Sabatier reaction will consume carbon dioxide and hydrogen as it produces methane which will further drive the WGS reaction towards the product side in accordance with Le Châtelier's principle. If one is to extract the kinetic parameters that describe the WGS reaction alone, then the conversion of carbon monoxide for a WGS

reaction process must be isolated from the contribution to the conversion of carbon monoxide due to the presence of the Sabatier reaction. The conversion due to the WGS reaction can therefore be recovered from the reported conversions as follows.

$$X_{CO,T} \equiv X_{CO,1} + X_{CO,2} \tag{2}$$

$$X_{CO,2} \equiv S_{CH_4} * X_{CO,T} \tag{3}$$

Where $X_{CO,T}$ is the conversion of carbon monoxide reported; $X_{CO,1}$ and $X_{CO,2}$ are the conversions of carbon monoxide due to the WGS and the Sabatier reaction respectively. Note that in these derivations, selectivity was defined by the following relationship

$$S_{CH_4} = \frac{C_{CH_4}}{C_{CO}^{in} X_{CO,T}} \tag{4}$$

For experiments on ruthenium-based catalysts, this application of the selectivity data is crucial due to ruthenium's high methanation promotion. For other catalysts, e.g. platinum, however, methanation promotion is be minimal. Thus, the total conversion, $X_{CO,T}$, could then be used in the recovery of the kinetic parameters for those catalysts and adjusting the carbon monoxide conversion reported would not be necessary.

Equilibrium Constant

The equilibrium constant will be defined by Equation 5 as it is in the paper [13]

$$K_c = \frac{k_f}{k_b} \tag{5}$$

In order to obtain values for K_c at the temperatures of the experiments in the given data, the van't Hoff equation is applied. Values for K_c were calculated and correlated as

$$K_c = K_o \exp\left(-\frac{\Delta H_R}{R}\left(\frac{1}{T} - \frac{1}{T^{ref}}\right)\right) \tag{6}$$

$$\ln(K_c) = -\frac{\Delta H_R}{R}\left(\frac{1}{T} - \frac{1}{T^{ref}}\right) + \ln(K_o) \tag{7}$$

To retrieve the K_o and $-\frac{\Delta H_R}{R}$ parameters necessary for calculating K_c at the temperatures of the given data, a linear regression was performed on the data plotted by Equation 7. The data and correlation can be found in the Appendix.

The Simplified Model

Equation 8 is the model proposed in the paper [13]

$$-r_{CO}^{w} = k_f^{w} P_{CO} + k_b^{w} P_{CO_2} \tag{8}$$

For this *Simplified Model*, the partial pressures of water and hydrogen are assumed to be constant at the inlet values and embedded in k_f and k_b respectively. This can be illustrated in the following rate equation. Concentrations are instead used to eliminate the need for a recurring conversion factor.

$$-r_{CO} \approx \overline{k}_f C_{CO} - \overline{k}_b C_{CO_2} \approx \left(k_f C_{H_2O}^{in}\right) C_{CO} - \left(k_b C_{H_2}^{in}\right) C_{CO_2} \tag{9}$$

$$-r_{CO} \approx \left(k_f C_{H_2O}^{in}\right) C_{CO}^{in}\left(1 - X_{CO,1}\right) - \left(k_b C_{H_2}^{in}\right) C_{CO}^{in} X_{CO,1} \tag{10}$$

This derivation is performed on a rate equation using concentrations while Equation 1 is in terms of partial pressures. Applying the design equation for a PFR and rewriting the equation to solve for conversion with respect to time, we get Equation 11 which is the starting point for our derivations.

$$\frac{dF_{CO}}{dV} = -r_{CO} \tag{11}$$

$$\frac{dX_{CO,1}}{dt} \approx \left(k_f C_{H_2O}^{in}\right)\left(1 - X_{CO,1}\right) - \left(k_b C_{H_2}^{in}\right)X_{CO,1} \tag{12}$$

To continue the derivation, identify the pseudo-constants as Equations 13 and 14

$$\overline{k}_f = k_f C_{H_2O}^{in} \qquad \overline{k}_b = k_b C_{H_2}^{in} \tag{13-14}$$

then divide both sides of the equation by C_{CO}^{o}.

$$\frac{dX_{CO,1}}{dt} \approx \overline{k}_f\left(1 - X_{CO,1}\right) - \overline{k}_b X_{CO,1} \tag{15}$$

$$\frac{dX_{CO,1}}{dt} \approx \overline{k}_f - (\overline{k}_f + \overline{k}_b)X_{CO,1} \tag{16}$$

$$\frac{dX_{CO,1}}{dt} \approx \overline{k}_f\left(1 - \alpha X_{CO,1}\right) \qquad \text{with } \alpha = 1 + \frac{\overline{k}_b}{\overline{k}_f} \approx 1 + \frac{1}{K_c} \tag{17-18}$$

The assumption that K_c is equal to $\frac{\overline{k}_f}{\overline{k}_b}$ is fundamental to how the parameters were retrieved in the paper this data was collected from. In Equation 19, it can be seen that constant concentrations of water and hydrogen are inconsistently embedded in K_c.

$$K_c = \frac{k_f C_{H_2O}^{in}}{k_b C_{H_2}^{in}} \tag{19}$$

Integrating Equation 17 yields the following solution for $\overline{k}_f$. This can then be rearranged to yield Equation 21 which is the model presented in the paper [13]

$$-\frac{1}{\alpha\tau}\ln\left(1 - \alpha X_{CO,1}\right) = \overline{k}_f \tag{20}$$

$$X_{CO,1}(\tau) = \frac{\overline{k}_f}{(\overline{k}_f + \overline{k}_b)}\left[1 - e^{(\overline{k}_f + \overline{k}_b)\tau}\right] \quad (21)$$

Values for average residence time can be calculated from volume of the reactor and the volumetric flow rate data. With the volumetric flow rate given in units of SLPM, an adjustment for temperature and pressure is necessary. The volume of the reactor was calculated using the catalyst support monolith dimensions and void fraction reported by Wheeler et al [13].

$$\tau = \frac{V\varepsilon}{Q^o}\left(\frac{T^o}{T}\right) \div 60\frac{s}{min} \quad (22)$$

Retrieving Parameters

The integration step for all models requires that both sides of Equation 17 be divided by a rewritten form of $-r_{CO}$. When $X_{CO,1}$ reaches equilibrium values, the value of $-r_{CO}$ becomes 0. We cannot divide by 0 and therefore cannot use data points at or beyond equilibrium to calculate $\overline{k}_f$'s for the *Simplified Model* or any other model discussed henceforth. Additionally, for ruthenium, the first two points in the data set cannot be used to retrieve $\overline{k}_f$'s due to their temperature difference from the third data point and all other data points. This temperature difference translates to a gap in the data set which makes the trend between points 2 and 3 unpredictable. However, *all* data points will be used when comparing fits in Chapter IV.

Values for k_f (or $\overline{k}_f$ for the *Simplified Model*) can now be calculated for each data point. A linear regression is performed on these calculated k_f values against an adjusted temperature. The intercept of the line, ln k_o, can then be used in the Arrhenius equation to solve for the pre-exponential factor for the forward reaction.

$$\ln k_f = \ln k_o + \frac{E_f}{R}\left(\frac{1}{T} - \frac{1}{T^{ref}}\right) \tag{23}$$

$$A_f = e^{\left(\ln k_o + \frac{E_f}{R}\frac{1}{T^{ref}}\right)} \tag{24}$$

For the *Simplified* and *Excess Model,* the Arrhenius equation and adjustment from the reference temperature will not yield the native parameters but pseudo parameters (see Equations 25-26).

$$\ln \overline{k}_f = \ln \overline{k}_o + \frac{\overline{E}_f}{R}\left(\frac{1}{T} - \frac{1}{T^{ref}}\right) \tag{25}$$

$$\overline{A}_f = e^{\left(\ln \overline{k}_o + \frac{\overline{E}_f}{R}\frac{1}{T^{ref}}\right)} \tag{26}$$

The assumption applied in Equation 18 of the *Simplified Model* was rewritten to see whether or not the parameters in the paper could be retrieved. This next model can be referred to as the *Excess Model*, for it still assumes constant concentrations of water and hydrogen but maintains the original definition of K_c described by Equation 5.

The Excess Model

For the derivation of the *Excess Model*, one can begin with Equation 27 and redefine α as Equation 28 to isolate the inlet concentrations of water and hydrogen from the definition of K_c

$$\frac{dX_{CO,1}}{dt} \approx \overline{k}_f\left(1 - \alpha X_{CO,1}\right) \qquad \text{with } \alpha = 1 + \frac{\overline{k}_b}{\overline{k}_f} \approx 1 + \frac{C_{H_2}^{in}}{C_{H_2O}^{in} K_c} \tag{27-28}$$

Although this model more appropriately applies the simplification made by the *Simplified Model,* it is not going to be suitable for retrieving the kinetics if we want to apply those kinetics to our waste gasification process. In order to account for the change

in the concentrations of water and hydrogen, the originally proposed power-law model (Equation 1) is written in terms of concentration and no species are assumed constant along the length of the reactor.

The Bimolecular Model

The retrieval of the kinetics for this scenario begins with application of the reactor design equation for a PFR (Plug Flow reactor) which describes the behavior of what is actually a PBR (Packed-bed reactor). Combining the design equation and Equation 29 brings us to the Equation 30.

$$-r_{CO} = k_f C_{CO} C_{H_2O} - k_b C_{CO_2} C_{H_2} \tag{29}$$

$$\frac{dC_{CO}}{dt} = k_f C_{CO} C_{H_2O} - k_b C_{CO_2} C_{H_2} \tag{30}$$

Using stoichiometric tables, the reactor design equation in terms of the carbon monoxide conversion becomes Equation 31. The feed of carbon dioxide is zero and the definition of K_c is applied to yield Equation 32

$$\frac{dX_{CO,1}}{dt} = k_f\left(1 - X_{CO,1}\right)\left[C_{CO}^{in}\left(\theta_B - X_{CO,1}\right)\right] - k_b\left(\theta_C + X_{CO,1}\right)\left[C_{CO}^{n}\left(\theta_D + X_{CO,1}\right)\right] \tag{31}$$

$$\frac{dX_{CO,1}}{dt} = k_f\left[\left(1 - X_{CO,1}\right)\left[C_{CO}^{in}\left(\theta_B - X_{CO,1}\right)\right] - \frac{1}{K_c} X_{CO,1}\left[C_{CO}^{in}\left(\theta_D + X_{CO,1}\right)\right]\right] \tag{32}$$

For the conditions of Wheeler's data, the feed ratios of water and hydrogen with respect to carbon monoxide are 4 and 2 respectively while no carbon dioxide is fed in any of the experiments [13]. The right side of Equation 6 can now take the form of a quadratic equation as shown below, where definitions of a, b, and c are all specific to the feed

conditions used to obtain the data reported but can be easily rederived for different feed conditions where carbon dioxide is introduced.

$$a = C_{CO}^{in}\left(1 - \frac{1}{K_c}\right) \qquad b = C_{CO}^{in}\left(-1 - \theta_B - \frac{\theta_C}{K_c}\right) \qquad c = \theta_B C_{CO}^{in} \tag{33-35}$$

$$aX_{CO,1}^2 + bX_{CO,1} + c = 0 \tag{36}$$

$$\int_0^{X_{CO}} \frac{dX_{CO,1}}{aX_{CO,1}^2 + bX_{CO,1} + c} = k_f \int_0^{\tau} dt \tag{37}$$

This integral can be solved analytically, i.e.

$$\frac{1}{a\tau(p-q)} \ln\left[\left(\frac{q}{p}\right)\left(\frac{X_{CO,1} - p}{X_{CO,1} - q}\right)\right] = k_f \tag{38}$$

Where p and q are the roots of the quadratic (Equation 12).

The forward and backward reaction parameters were then used to solve for conversion and the results were compared to the experimental data via a coefficient of determination

$$RSS = \sum_{i=1}^{n} \left(X_{CO,1}^{Exp} - X_{CO,1}^{pred}\right)^2 \tag{39}$$

$$TSS = \sum_{i=1}^{n} \left(X_{CO,1}^{Exp} - \overline{X}_{CO,1}^{pred}\right)^2 \tag{40}$$

$$R^2 = 1 - \frac{RSS}{TSS} \tag{41}$$

Summary of Models

The partial pressures of water and hydrogen are removed from the *Simplified Model* and the *Excess Model* on account of the assumption that they are nearly constant.

While this assumption eventually proved to be acceptable given the particular experimental setup and feed conditions used to collect this data, it could not be anticipated that these assumptions would be appropriate for other processes. This meant that the kinetic parameters calculated according to this model for the WGS reaction would not be applicable to the process in our laboratory or any other process where the amounts of water and hydrogen were subject to change. The *Bimolecular Model*, on the contrary, is expected to be applicable to a much wider variety of processes involving the water-gas shift reaction including the process in our laboratory.

In Chapter IV, the models will be tested and compared to tell the story of why the *Simplified Model* was used in the literature and why the *Bimolecular Model* originally was not.

Selectivity of Oxidation

The oxidation fraction when calculating the maximum potential methane production for the experiments is assumed to be zero. Of course, this will not always be the case. Therefore it is of interest to investigate the selectivity of the liquid-phase oxidation reactions. In other words: how does the polymer choose between conversion to carbon dioxide vs. carbon monoxide?

We can retrieve the reaction kinetics for the following reactions from the experimental data gathered by our GC.

$$(C_2H_4)_n + 3nO_2 \rightarrow 2nCO_2 + 2nH_2O \quad (42)$$

$$(C_2H_4)_n + 2nO_2 \rightarrow 2nCO + 2nH_2O \quad (43)$$

First, we define selectivity as the following where A is the polyethylene monomer.

$$S_i = \frac{N_i}{N_A^o} \tag{44}$$

Gasification is a complex reaction process with both series and parallel reactions occurring simultaneously. We must recognize that the definition presented as Equations 44 hold for both parallel, series, and reversible reactions.

Applying this concept to the reaction pathways for polyethylene gasification, we can recover the reaction rates of the oxidation reactions. For the following relationships, the reactions of polyethylene are numbered as follows. V_1 and V_2 refer to the liquid and gas volumes in the batch reaction respectively. The values of these volumes are approximate due to unknown headspace in the reactor apparatus above the vessel and VLE behavior throughout the reaction.

1) $$(C_2H_4)_n + 3nO_2 \rightarrow 2nCO_2 + 2nH_2O$$

2) $$(C_2H_4)_n + 2nO_2 \rightarrow 2nCO + 2nH_2O$$

3) $$CO + H_2O \leftrightarrow CO_2 + H_2$$

4) $$CO_2 + 4H_2 \leftrightarrow CH_4 + 2H_2O$$

$$N_A^o \frac{dS_{CO}}{dt} = 2r_2V_1 - r_3V_2 \qquad N_A^o \frac{dS_{CH_4}}{dt} = r_4V_2 \tag{45-46}$$

$$N_A^o \frac{dS_{CO_2}}{dt} = 2r_1V_1 + r_3V_2 - r_4V_2 \qquad N_A^o \frac{dS_{H_2}}{dt} = r_3V_2 - 4r_4V_2 \tag{47-48}$$

By taking these equations and combining them, we can retrieve the rates of the oxidation reactions.

$$\frac{dS_{CO}}{dt} + \frac{dS_{H_2}}{dt} + 4\frac{dS_{CH_4}}{dt} = 2r_2V_1 - r_3V_2 + r_3V_2 - 4r_4V_2 + 4r_4V_2 \tag{49}$$

$$\frac{dS_{CO_2}}{dt} - \frac{dS_{H_2}}{dt} - 3\frac{dS_{CH_4}}{dt} = 2r_1V_1 + r_3V_2 - r_4V_2 - r_3V_2 + 4r_4V_2 - 3r_4V_2 \quad (50)$$

Remaining reaction rates of the WGS and Sabatier cancel to leave only the rates of the oxidation reactions.

$$N_A^o\left(\frac{dS_{CO}}{dt} + \frac{dS_{H_2}}{dt} + 4\frac{dS_{CH_4}}{dt}\right) = 2r_2V_1 \quad (51)$$

$$N_A^o\left(\frac{dS_{CO_2}}{dt} - \frac{dS_{H_2}}{dt} - 3\frac{dS_{CH_4}}{dt}\right) = 2r_1V_1 \quad (52)$$

One can then quantify the selectivity of oxidation for the polyethylene monomer in the waste gasification process at each temperature of reaction. The optimal value of this selectivity for methane generation would then be 0.

$$S_{co_2/co} = \frac{r_{co_2}}{r_{co}} = \frac{k_1}{k_2} \quad (53)$$

The concentrations of polyethylene cancel leaving only the ratio of the rate constants. If this information can be recovered for a range of temperatures, then the kinetic parameters of the liquid-phase oxidation reactions could eventually be recovered. If the orders of the reactions differ, then the ratio of the reactions will not be constant with respect to temperature. Thus, an additional step will be required to recover the selectivity of oxidation for the temperature of interest. The rate laws can be identified as the following with oxygen concentration constant at saturation in the liquid phase.

$$r_1 = k_1C_A^{n_1} \quad (54)$$

$$r_2 = k_2C_A^{n_2} \quad (55)$$

Dividing Equation 54 by 55 and taking the natural logarithm yields Equation 56.

$$\ln\frac{r_{CO_2}}{r_{CO}} = (n_1 - n_2) * \ln\left[\frac{N_A^o}{V_1}(1 - X_A)\right] + \ln\frac{k_1}{k_2} \quad (56)$$

Plotting the data according to Equation 56 yields the slope and intercept which describe the difference in the orders of reactions and the ratio of the reaction rate constants respectively.

In the future, the pre-exponential factors and the activation energies of the reactions can be found by isolating k_1 and k_2 from the ratio and plotting them against adjusted temperatures.

Combining with the design equation for a batch reactor and linearizing the resulting formula, the rate constant at a specific temperature can be obtained. Consumption of A is a consequence of both reactions 1 and 2. Equation 74 results and can be rearranged to solve for the rate constant of the carbon dioxide oxidation reaction.

$$\frac{dN_A}{dt} = -r_A V_1 \quad (72)$$

$$-r_A = k_1 C_A + k_2 C_A \quad (73)$$

$$\frac{dX_A}{dt} = -k_1\left(1 + \frac{k_2}{k_1}\right)(1 - X_A) \quad (74)$$

CHAPTER III

EXPERIMENTAL

From Proof to Optimization

Our laboratory's efforts began with a proof of concept. High fidelity waste simulant (HFWS), a fibrous material that mimics the elemental composition of the International Space Station waste stream, was heated to 310 ℃ in the wet thermal batch gasification process. Analysis of product gas samples at the end of the run proved the presence of methane, hydrogen, carbon monoxide, and carbon dioxide. Wet thermal catalytic gasification works as a process that can produce useful products from International Space Station waste stream compositions. Now, we want to make possible the optimal design of a waste gasification system. While it is unlikely to recover any reaction kinetics from HFWS experiments, batch reaction data from individual polymers may make recovery of reaction kinetics possible.

Apparatus and Procedures Overview

Reaction Conditions	
Reaction Temperatures (˚C)	310-320 ± 1
Reaction Pressures (psia)	1400 – 1800 ± 1
Reactor Volume (mL)	100 ± 1
Stirrer Speed (rpm)	370-390 ± 1

Table 1: The conditions of the reactor once desired temperature was reached. Reactor volume is approximate due to unknown headspace in valve ports at top of vessel.

Heating was done in step ramps to prevent chemical reaction from occurring before reaching desired temperatures (from room temperature to 185 ˚C, then 220 ˚C, then 250 ˚C, then 275 ˚C, then reaction temperature). Reactions ended when the heat jacket was removed and water batch cooling of the reactor vessel was initiated. The stirrer was left on to aid in cooling during this phase. Cooling water was also run continuously through the cooling jacket at the base of the stirrer magnetic drive from heating phase to cooling phase of the reactor vessel. Blank reactions (catalyst and water only) were run in between reactions to remove any possible residuals which eluded standard cleaning procedures. Figure 3 shows the experimental setup.

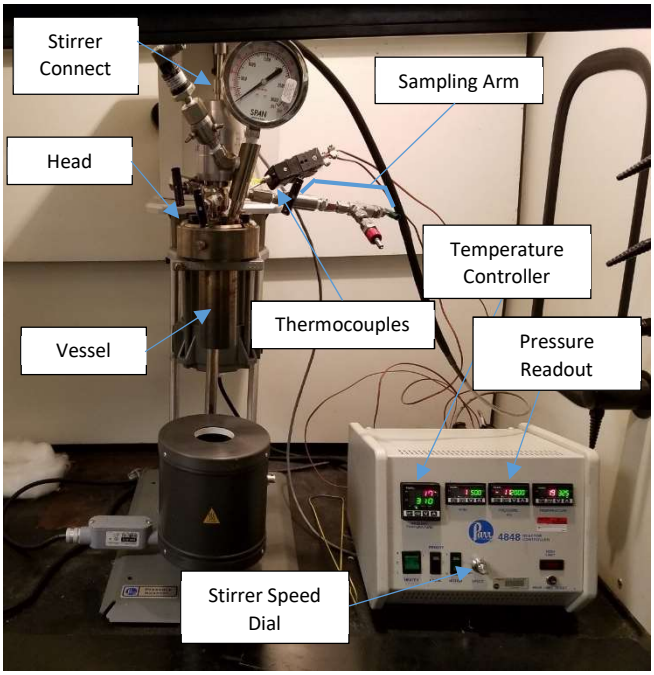

Figure 3: Photo of reactor setup with controller and important components identified

Reactor Loading	
Temperature (˚C)	17-26 ± 1
Air Pressure (psia)	139 ± 1
DI (deionized) Water (mL)	20 ± 0.1
Polyethylene (g)	0.060 ± 0.001
5 wt% Ruthenium on Alumina (g)	0.060 ± 0.001

Table 2: Batch reactor loading conditions for polyethylene gasification on ruthenium-based catalyst. Ranges in temperature are due to seasonal weather

Loading of polymer was stoichiometric based on air pressure (moles oxygen) with respect to carbon dioxide in the first oxidation reaction and DI water was loaded in excess at 20 mL to submerge the stirrer (Polymer loading calculations are discussed in detail at the end of the chapter).

Sampling was done using 300 mL Swagelok portable cylinders which were prepared with silica gel to adsorb water. Silica gel was pre-saturated with Matheson Tri-Gas standard gas mixtures at a high carbon monoxide composition to saturate the silica gel with carbon monoxide and prevent any absorbance of carbon monoxide produced in the batch reactions. Sampling was done when the reactor controller no longer displayed a climb in temperature upon stirrer shut-off and when the reactor temperature remained below 50 ˚C. A GC-TCD (Gas Chromatograph-Thermal Conductivity Detector) was used for analysis of the product gas and 1 mL injections were made using a Hamilton 1 mL syringe. Integration of peaks in the GC software was done manually. Figure 4 is a depiction of the interior of the process. Figure 5 is a schematic which illustrates the overall experimental process and the main components of the apparatus.

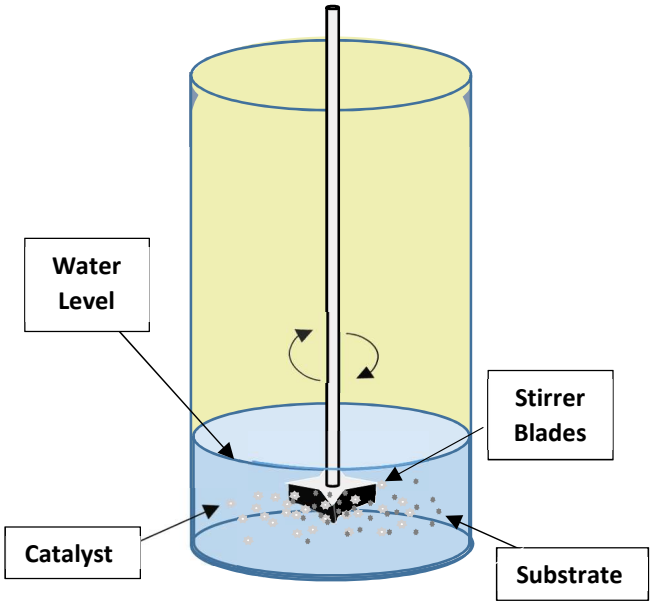

Figure 4: A depiction of the interior of the batch reactor for the wet thermal catalytic gasification process. Not to scale.

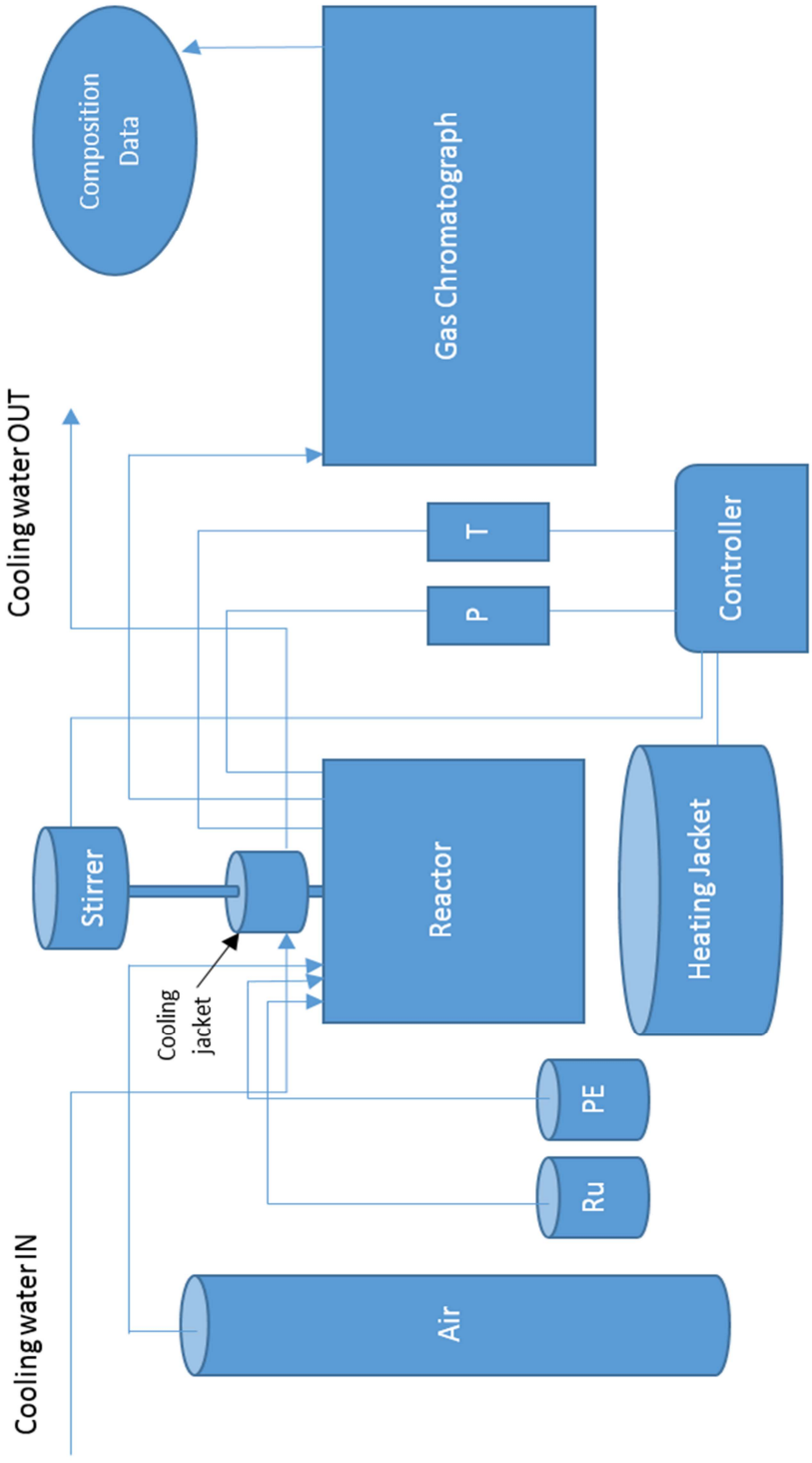

Figure 5: Schematic of overall experimental process. Heating Jacket is raised over reactor during reactions. T and P represent signals to controller. Ru and PE are ruthenium-based catalyst and polyethylene respectively.

Loading Material Specifications

Polyethylene (Medium density)	
Appearance	Light grey powder
Melting point/freezing	109-111 ˚C (228-232 ˚F)
Flammability	May form combustible dust concentrations in air
Relative density	0.94 g/mL at 25 ˚C (77 ˚F)
Hazard Rating	0
CAS-No.	9002-88-4

Table 3: Polyethylene was obtained from Sigma-Aldrich. Above is the relevant material information

Platinum on alumina - 5 wt. % loading (± 0.2%)	
Appearance	Grey to Black Powder
Health Hazard Rating	2
Aluminum oxide CAS-No.	1344-28-1
Platinum CAS-No.	7440-06-4

Table 4: Platinum was obtained from Sigma-Aldrich. Above is the relevant material information.

Ruthenium on alumina - 5 wt. % loading (± 0.2%)	
Appearance	Grey to Black Powder
Hazards	Non-hazardous
Aluminum oxide CAS-No.	1344-28-1
Ruthenium CAS-No.	7440-18-8

Table 5: Ruthenium was obtained from Sigma-Aldrich. Above is the relevant material information.

Air, Compressed	
Density	1,200 kg/m^3 at 21.1 ˚C, 101.325 kPa
Hazards	Non-Flammable, Non-Poisonous
Carbon Dioxide	< 1 ppm
Carbon Monoxide	< 1 ppm
THC	< 0.1 ppm
Water	< 2 ppm
Oxygen	20-22% (Assume to be 21%)
CAS-No.	132259-10-0

Table 6: Compressed Air was obtained from Matheson Tri-Gas. Above is the relevant material information.

GC Calibration and Outlier Analysis

Calibration standards were purchased from Matheson Tri-Gas as mixtures with varying compositions of carbon dioxide, carbon monoxide, methane, and hydrogen with

either helium or nitrogen as balance. Oxygen was also included in some of the standards but could not be modeled by a linear regression and thus could not be quantified for experiments (See Appendix for Standard Specs). Below is Figure 6, an example curve (See Appendix for all Curves).

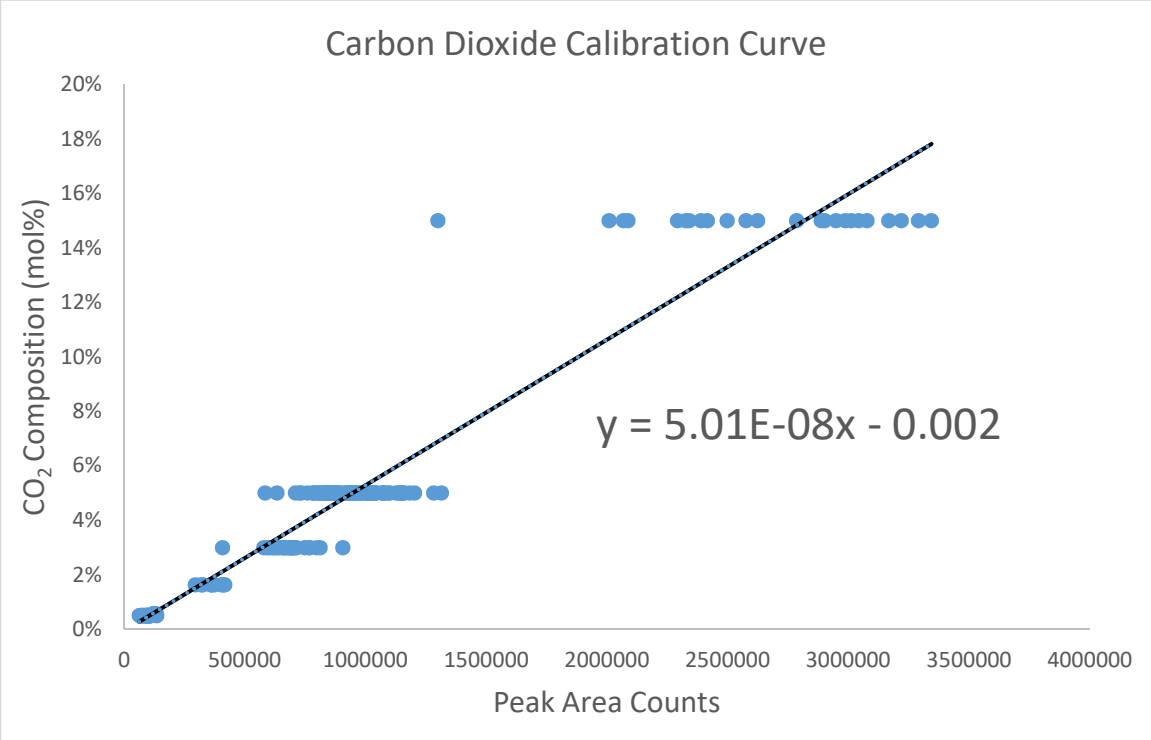

Figure 6: Above is calibration curve for carbon dioxide. Data points come from integration of CO_2 peaks in standard gas mixtures. The linear regression was used to convert peak area counts from experimental reaction runs into molar compositions. This analysis was also done on carbon monoxide, methane, hydrogen.

As was the case with the batch reaction product gases, calibration standards were loaded into 300 mL sample cylinders. Silica gel was not introduced, however, because there was no reason to suspect moisture in the research-grade calibration mixtures. Sample cylinders loaded with standard or experimental product gas were considered unreliable after 1 day of storage therefore as many injections were made as possible on after the cylinder's loading.

Standards would be injected and run through the GC anywhere from 8 to 20 times in a row to provide a larger pool of data for statistical analysis. Processing this large quantity of calibration points involved a quantile analysis. Each set of points for a given standard gas mixture was divided into quartiles. *f*, the Interquartile Range, was also calculated.

$$Q_1 \equiv \text{The median of the lowest 25\% of the data set}$$

$$Q_3 \equiv \text{The median of the highest 25\% of the data set}$$

$$f = Q_3 - Q_1 \tag{75}$$

The lower and upper fences were defined as follows:

$$\text{Lower Fence} \equiv Q_1 - 3 * f \tag{76}$$

$$\text{Upper Fence} \equiv Q_3 + 3 * f \tag{77}$$

If a point in the data set had a GC peak area count below the Lower Fence or above the Upper Fence, that point was removed from the calibration curve. That is to say that the peak area counts for every component in that GC injection were removed regardless of which component proved to be an outlier. In Figure 7, the carbon dioxide peak area counts for all of the injections of the product gas in Experiment 126 are shown.

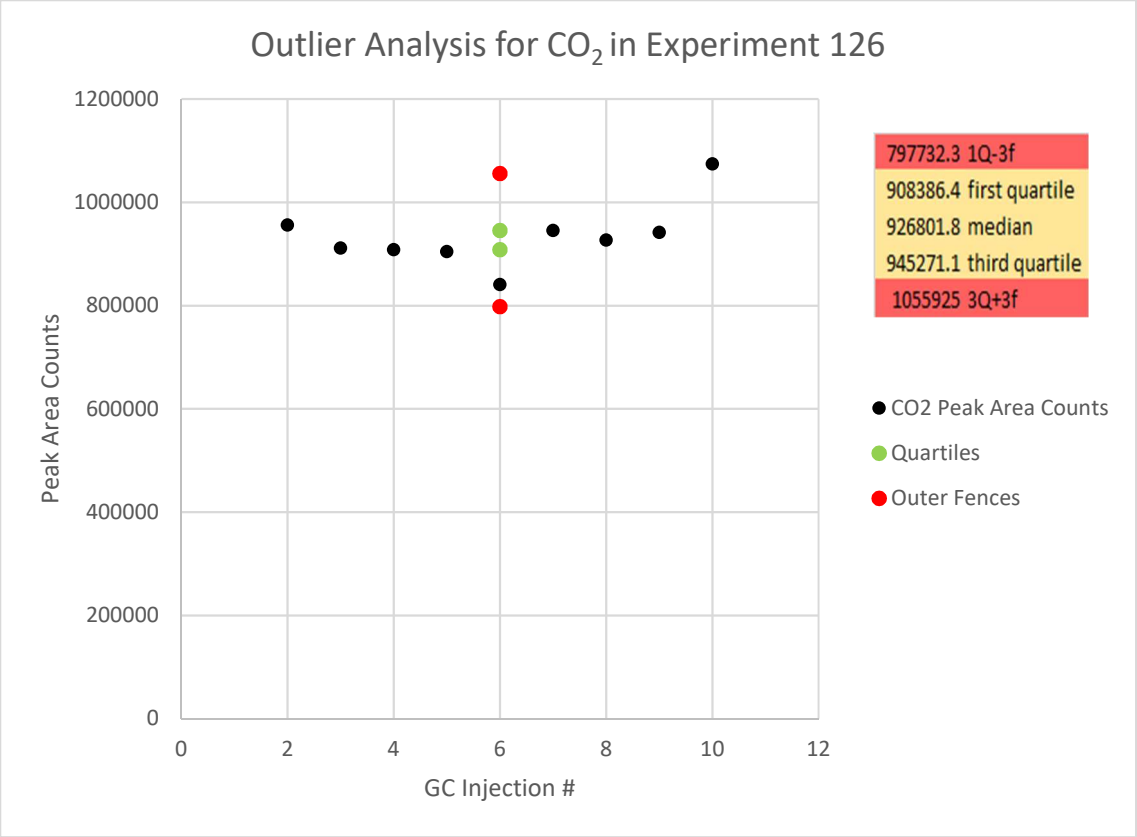

Figure 7: The above Example Plot illustrates the method of outlier analysis discussed in the text. Green circles correspond to the first and third quartile of the data set. The red circles correspond to the upper and lower fences of the data set. The first injection is absent from the plot because all first injections proved to be outliers.

CH_4	Peak Area
2	15387.6
3	14399.8
4	14482.5
5	15045.9
6	13070
7	15242.9
8	14964.6
9	14779.9
10	17046.9

CH_4	
f	760.4
FIRST Q - 3f	12201.3
FIRST Q	14482.5
MEDIAN	14964.6
THIRD Q	15242.9
THIRD Q + 3f	17524.1

CO_2	Peak Area
2	956149.8
3	911348.1
4	908386.4
5	904268.1
6	840766.6
7	945271.1
8	926801.8
9	941804
10	1074166.3

CO_2	
f	36884.7
FIRST Q - 3f	797732.3
FIRST Q	908386.4
MEDIAN	926801.8
THIRD Q	945271.1
THIRD Q + 3f	1055925

Figure 8: The above spreadsheet is an example of the outlier analysis for Experiment 126. The quartile values revealed that the CO_2 peak in Injection #10 is an outlier (See red highlighted cell). Because all components are present in that injection, all components are ignored if one component of the injection is outside the outer fences (See red font cell in CH_4 section). Only green font cells are included in the calculation of the average peak area (which translates to average composition of the species) for the experiment. CO and H_2 are not shown here for sake of simplicity.

The last injection (Injection #10) has a peak area count of 1074166 which exceeds the Upper Fence of 1055925 for this data set. The peak data for all components in Injection #10 will be omitted from the average peak area calculation as can be seen in Figure 8 below.

Calibration standards were run regularly and points were added to the calibration curves over time. As was seen in Figure 7, this method of outlier analysis was also conducted on the experimental data sets. For reasons unknown, the first injection of any standard or sample consistently proved to be far below every other injection in the set and was thus removed as a rule.

Once the average peak area count is determined for each component, the calibration curve is used to calculate the molar composition in the sample cylinder. Because the sample cylinder is diluted with helium at atmospheric pressure, this molar composition must be adjusted to reflect the percentage of the component in the reactor.

$$y_i = (m_i x_i + b_i) * \left(\frac{n_{tot}}{n_{sam}}\right) \tag{78}$$

$$n_{sam} = \frac{P^{sam} * V_{cyl}}{R * T^{cyl}} \tag{79}$$

$$n_{He} = \frac{P^{He} * V_{cyl}}{R * T^{cyl}} \tag{80}$$

$$n_{tot} = n_{sam} + n_{He} \tag{81}$$

Implementation of Blank Protocol

In an effort to increase the accuracy of our data, we ran an experiment to evaluate the effectiveness of our reactor cleaning process. After several polyethylene gasification experiments were performed in the reactor with the standard cleaning procedure carried out, a blank reaction was run. The blank was loaded with 60 mg of ruthenium, 60 mg of platinum, and 20 mL of water but no substrate. It was hypothesized that if there was any residual polyethylene substrate from a previous reaction, the catalyst would oxidize it and gas phase products would be seen in the GC analysis. The blank was run for 16 hours to ensure plenty of time for gasification. GC analysis revealed approximately 500000 area counts of carbon dioxide which, according to our calibration curve (Figure 6), corresponds to between 2 and 3 mol% carbon dioxide. This is significant when only 21% of the system's gas phase can be syngas due to the presence of nitrogen. These results indicated a presence of residual, un-gasified polyethylene that was eluding the cleaning procedure.

At first, it was desired to run one blank after every two subsequent gasification experiments. This would greatly conserve time and labor. However, following the completion of Experiments 113 and 114, a blank run with platinum and ruthenium catalyst revealed approximately 400000 area counts for the carbon dioxide peak indicating concentrations upwards of 2 mol% which we considered too high to have confidence in the concentrations of Experiment 114. With a carbon dioxide signal of this magnitude, the results for the second reaction could be compromised by the presence of residual substrate from the first reaction. In order to avoid this uncertainty, the protocol was adjusted to one blank after every gasification experiment. Gasification experiments

following this investigation would always be followed by a blank run with ruthenium catalyst to clean the reactor. Any experiments that didn't follow this protocol were omitted from the final results.

We then decided to study the effect of using ruthenium vs. platinum as a cleaning catalyst. A blank with only ruthenium catalyst was run following an 18 h polyethylene gasification experiment. The carbon dioxide peak contained approximately 300000 area counts showing that appreciable oxidation of the residual substrate was still possible without the presence of both catalysts.

In an effort to be further certain of the effectiveness of the cleaning power of just one blank, an experiment was run where two blank reactions would be run following a gasification experiment. If a single blank was sufficiently gasifying unwanted residuals, the second blank would yield little or no carbon dioxide. The first blank in this experiment gave GC results with carbon dioxide peaks of approximately 150000 area counts and the second experiment showed approximately 100000 area counts. This experiment was conducted approximately ten gasification experiments after the initial implementation of the blank run protocol. Knowing that, the low signal of approximately 150000 area counts for the carbon dioxide peak of the first blank indicated to us that the nearly 600000 area count signals present in the first blank experiments could be attributed to the delayed implementation of this protocol in the wake of nearly 100 successive polyethylene gasification experiments. In other words, unwanted residual substrate had significantly more time to accumulate in the reactor than it did between the first blank reaction and blanks 11 and 12 which correspond to the approximate 150000 and 100000 area count carbon dioxide peak result values respectively (See Figure 9

below for clarification). This 30% decrease in carbon dioxide peak area count and a corresponding concentration of approximately 0.6 mol% in the product gas of the second blank for this experiment showed a great improvement from the nearly 3 mol% carbon dioxide present in the reactor to introduce significant error. Constraints on time and money also restrict the blank procedure to one blank and one catalyst after each experiment.

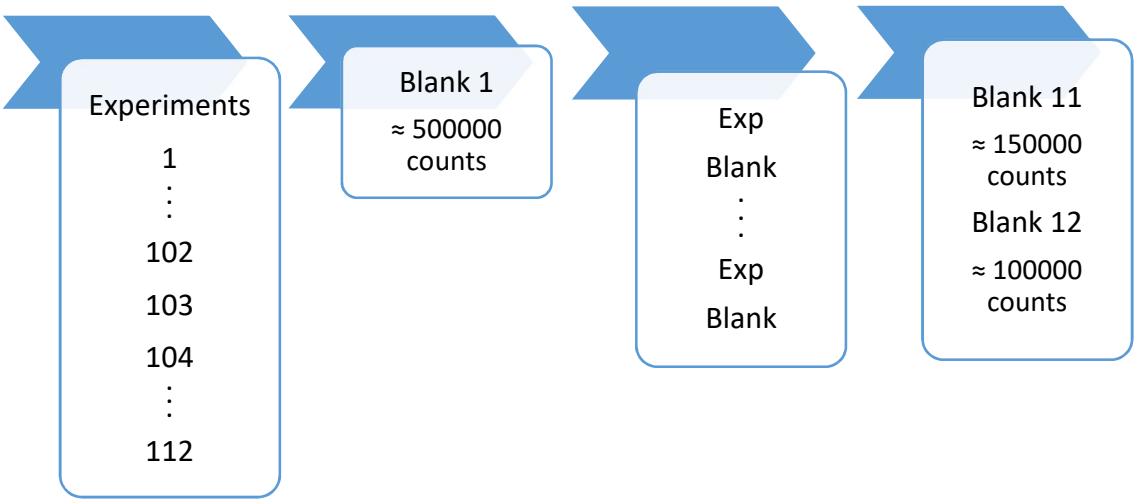

Figure 9: The above timeline highlights the quantity of reactions run without blanks prior to implementation of the blank procedure. This explains the abundance of CO_2 present in the first blank and the, by contrast, much lower CO_2 content in Blanks 11 and 12.

It should be noted that different conversions of the substrate would leave different amounts of solid carbon. A 2 h gasification experiment will leave a great deal more unreacted substrate than a 22 h gasification experiment that reaches nearly 100% conversion of the substrate. In other words, the 2 h gasification experiment will leave you with a "dirtier" reactor and thus a blank of a standard time and catalyst load will clean to different degrees following different experiments. To circumvent this problem, the knowledge gathered from experiment 122 was applied to the blank protocol procedure. In experiment 122, approximately 100% gasification was observed. This experiment

occurred at 320 ˚C for 17 hours. Based on this knowledge, we can run blanks under the same conditions to thoroughly eliminate unwanted residual substrate.

Determining Loading Mass

To determine the loading mass of substrate, an approximate maximum for the air pressure in the reactor during the loading phase was determined. It was found that a pressure of 139 psia could be reliably reproduced when loading from the air tank cylinder. With a target for a monomer count that would result in total oxygen consumption, the ideal gas law and the molar mass of polyethylene monomer were used to calculate the weight of polymer necessary for carrying the carbon dioxide oxidation reaction through to completion.

If the carbon monoxide oxidation reaction was chosen for the stoichiometric measurement, then there would not be enough oxygen present to allow for the monomer to select both of the oxidation pathways with equal opportunity. This would inhibit our ability to study the selectivity of these oxidation pathways by the monomer with respect to temperature and with respect to conversion of monomer. Regarding the calculation of the moles of oxygen, it was assumed that the temperature of the reactor vessel during the loading phase would always be 25 degrees C.

The Full Reaction Mechanism

When processing the GC data collected in our laboratory from batch gasification experiments, Percent Gasification is an important metric for analysis. This is equivalent to the conversion of the substrate. If we assume the Ideal Gas Law to be applicable then the following applies

$$X_{sub} = \frac{n_{C,prod}}{n_{C,loaded}} \tag{82}$$

$$n_{C,loaded} = c * n_{monomer} \tag{83}$$

$$n_{C,prod} = \frac{P^{col} * V_2}{R * T^{col}} * \left(y_{CO} + y_{CO_2} + y_{CH_4}\right) \tag{84}$$

With 20 mL of deionized water added to the reactor during the loading phase and knowing that the total volume of the vessel is 100 mL, a value of 80 mL is used in Equation 80. The uncertainty in this value of X_{sub} is subject to nearly every reading and/or measurement recorded in the experimental procedure except stirrer speed and the composition of hydrogen (See end of this Chapter as well as Appendix for propagation of uncertainty derivations).

Maximum Methane Yield

In order to have a validation metric, the maximum possible amount of methane that could be produced for a gasification experiment needs to be calculated. While it would be desirable to use simulation software to paint a more accurate picture of what can reasonably be expected of the system in the laboratory taking into account reaction reversibility and equilibrium limitations, the nature of the system makes this difficult. There are 3 phases present, at least 4 reactions, mixing effects, oxygen diffusion, and heat transfer phenomena to take into account. Avoiding these complications, we can make assumptions to calculate a maximum potential composition for each of the gaseous components. First, we assume that the polymer is completely gasified because that is the situation of interest. The following is an example for polyethylene.

$X_{C_2H_4} = 1.0$

The moles of carbon dioxide, carbon monoxide, and hydrogen are calculated following the oxidation phase.

$$n_{CO_2,1} = z * n_{PE} * \left(\frac{2\ mol\ CO_2}{1\ mol\ C_2H_4}\right) * X_{C_2H_4} \quad (85)$$

$$n_{CO,1} = (1 - z) * n_{PE} * \left(\frac{2\ mol\ CO}{1\ mol\ C_2H_4}\right) * X_{C_2H_4} \quad (86)$$

$$n_{O_2,1} = n_{O_2} - 0.5 n_{PE} \left(\frac{3\ mol\ O_2}{1\ mol\ C_2H_4} + \frac{2\ mol\ O_2}{1\ mol\ C_2H_4}\right) \quad (87)$$

The oxidation fraction, z, represents what fraction of the substrate will be converted to carbon dioxide as opposed to carbon monoxide. For the maximum methane production, z can be set to zero. Conversions of carbon monoxide and hydrogen are assumed to be 100% for the gas phase reactions. The WGS is then assumed to take place in the absence of the Sabatier reaction and the moles of carbon dioxide and hydrogen produced are calculated.

X_{CO} = 1.0

$$n_{CO_2,2} = n_{CO_2,1} + n_{CO,1} * \left(\frac{1\ mol\ CO_2}{1\ mol\ CO}\right) * X_{CO} \quad (88)$$

$$n_{H_2,2} = n_{CO,1} * X_{CO} \quad (89)$$

Finally, the Sabatier reaction is assumed to take place after the oxidation reactions and the WGS reaction have taken place. Conversion of hydrogen is 100%

X_{H_2} = 1.0

$$n_{CO_2,3} = n_{CO_2,2} - n_{H_2,2} * \left(\frac{1\ mol\ CO_2}{4\ mol\ H_2}\right) * X_{H_2} \quad (90)$$

$$n_{CH_4} = n_{H_2,2} * \left(\frac{1\ mol\ CO_2}{4\ mol\ H_2}\right) * X_{H_2} \quad (91)$$

Knowing the loading conditions for a given experiment, these calculations can provide us with an absolute maximum for the production of methane which can be useful for determining experimental consistency.

Determining Uncertainty

Error propagation equations were used to produce the error bars for the results presented in this Thesis. The equations for the uncertainties of all final results are shown below. The derivations can be found in the Appendix.

$$\omega_{X_{C_2H_4}} = \sqrt{\begin{matrix}\left(\frac{dX_{C_2H_4}}{dP^{col}} * \omega_{P^{col}}\right)^2 + \left(\frac{dX_{C_2H_4}}{dT^{col}} * \omega_{T^{col}}\right)^2 + \left(\frac{dX_{C_2H_4}}{dy_{CO}} * \omega_{y_{CO}}\right)^2 \\ + \left(\frac{dX_{C_2H_4}}{dy_{CO_2}} * \omega_{y_{CO_2}}\right)^2 + \left(\frac{dX_{C_2H_4}}{dy_{CH_4}} * \omega_{y_{CH_4}}\right)^2 + \left(\frac{dX_{C_2H_4}}{dm_A} * \omega_{m_A}\right)^2 \\ + \left(\frac{dX_{C_2H_4}}{dV_2} * \omega_{V_2}\right)^2\end{matrix}} \quad (92)$$

$$\omega_{y_i} = \sqrt{\left(\frac{dy_i}{dm_i} * \omega_{m_i}\right)^2 + \left(\frac{dy_i}{dx_i} * \omega_{x_i}\right)^2 + \left(\frac{dy_i}{dP^{sam}} * \omega_{P^{sam}}\right)^2 + \left(\frac{dy_i}{db_i} * \omega_{b_i}\right)^2} \quad (93)$$

$$\omega_{S_i} = \sqrt{\left(\frac{dS_i}{dn_i} * \omega_{n_i}\right)^2 + \left(\frac{dS_i}{dN_A^o} * \omega_{N_A^o}\right)^2} \quad (94)$$

Figure 10 compares the quantities of each term in the equations just described. It is clear that the largest contribution to the uncertainty in the molar compositions comes from the standard deviation in the area counts for the injection data set per experiment.

% Gasification Uncertainty						
P React	T React	y CO	y CH4	y CO2	m subs	V_{React}
8.9E-06	1.8E-05	0.00013	0.00030	0.00033	5.4E-05	3.0E-05
H_2 Uncertainty						
m_i	x_i	P_{cyl}	b_i			
9.3E-08	6.3E-07	1.4E-08	2.7E-06			
CO Uncertainty						
m_i	x_i	P_{cyl}	b_i			
1.4E-08	1.9E-08	5.6E-12	2.4E-06			
CH_4 Uncertainty						
m_i	x_i	P_{cyl}	b_i			
7.9E-09	8.1E-09	5.9E-09	5.7E-06			
CO_2 Uncertainty						
m_i	x_i	P_{cyl}	b_i			
6.8E-07	2.3E-06	1.8E-07	3.1E-06			

Figure 10: Quantified contributions of the uncertainties of each term in the propagation of uncertainty for some of the key results. Calculations shown are for experiment 141 at 8.63 hours reaction time and 315 ˚C reaction temperature.

CHAPTER IV

RESULTS & DISCUSSION

This chapter will cover several topics as they relate to retrieving the kinetics for the reactions of waste gasification. First, the models analyzed for the water-gas shift (WGS) reaction will be compared and we will report the kinetic parameters for the reaction over ruthenium and platinum-based catalysts. Moving on to the data collected in *our* laboratory, we will evaluate the trends in the composition data for carbon dioxide, carbon monoxide, methane, and hydrogen. Next, selectivity data generated from this is used to recover values for the selectivity of liquid-phase oxidation at different temperatures. Kinetics for these reactions will not be available until data at more temperatures is collected.

Comparison Among the Models

Figure 11 shows the carbon monoxide conversion reported in the paper, and the conversions attributable to each of the gas-phase reactions: (1) the Water-Gas Shift (WGS), and (2) the Sabatier reactions.

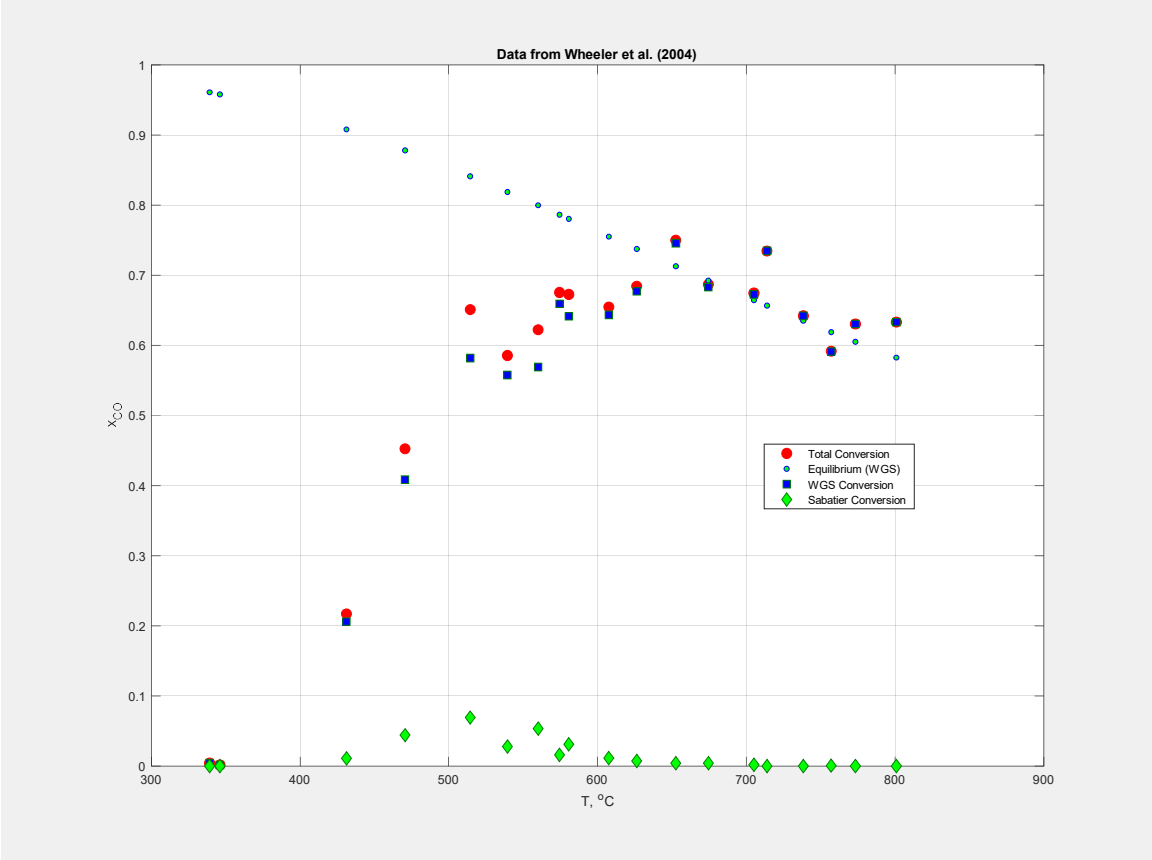

Figure 11: Conversions of carbon monoxide shown as a consequence of the water-gas shift alone and the series water-gas shift and Sabatier reactions. The contribution to the conversion of carbon monoxide by the Sabatier reaction alone is also shown and the equilibrium conversions for the water-gas shift are plotted. Total conversion data was collected by Wheeler et al.[13]

The conversion of carbon monoxide attributable to the WGS was next correlated using the *Simplified* and *Excess* models, as presented in Chapter II.

The parameters found for both models are presented in Table I below. One can clearly see that the pre-exponential factors found in our analysis differ from those reported by Wheeler et al [13] by more than an order of magnitude.

	Simplified Model	Reported w/ Data
$\overline{k}_{of}$	$2.5 \pm 0.2\ (s^{-1})$	$260\ (s^{-1})$
$\overline{E}_f$	$61.46 \pm 0.005041\ \left(\frac{kJ}{mol}\right)$	$80\ \left(\frac{kJ}{mol}\right)$
$\overline{k}_{ob}$	$0.93 \pm 0.072\ (s^{-1})$	Not reported
$\overline{E}_b$	$98.47 \pm 0.09847\ \left(\frac{kJ}{mol}\right)$	Not reported

Table 7: Comparison of the parameters derived from the Simplified Model derivations for the water-gas shift reaction. Data used to recover the parameters was adapted from Wheeler et al. (2004)

The relative error between the forward activation energy found using the *Simplified Model* and the one found in the original analysis by Wheeler et al. [13] is approximately 25%. The pre-exponential factors can clearly be seen to differ by nearly two orders of magnitude. Figure 12 & Figure 13 show the predictions of the parameters for the WGS.

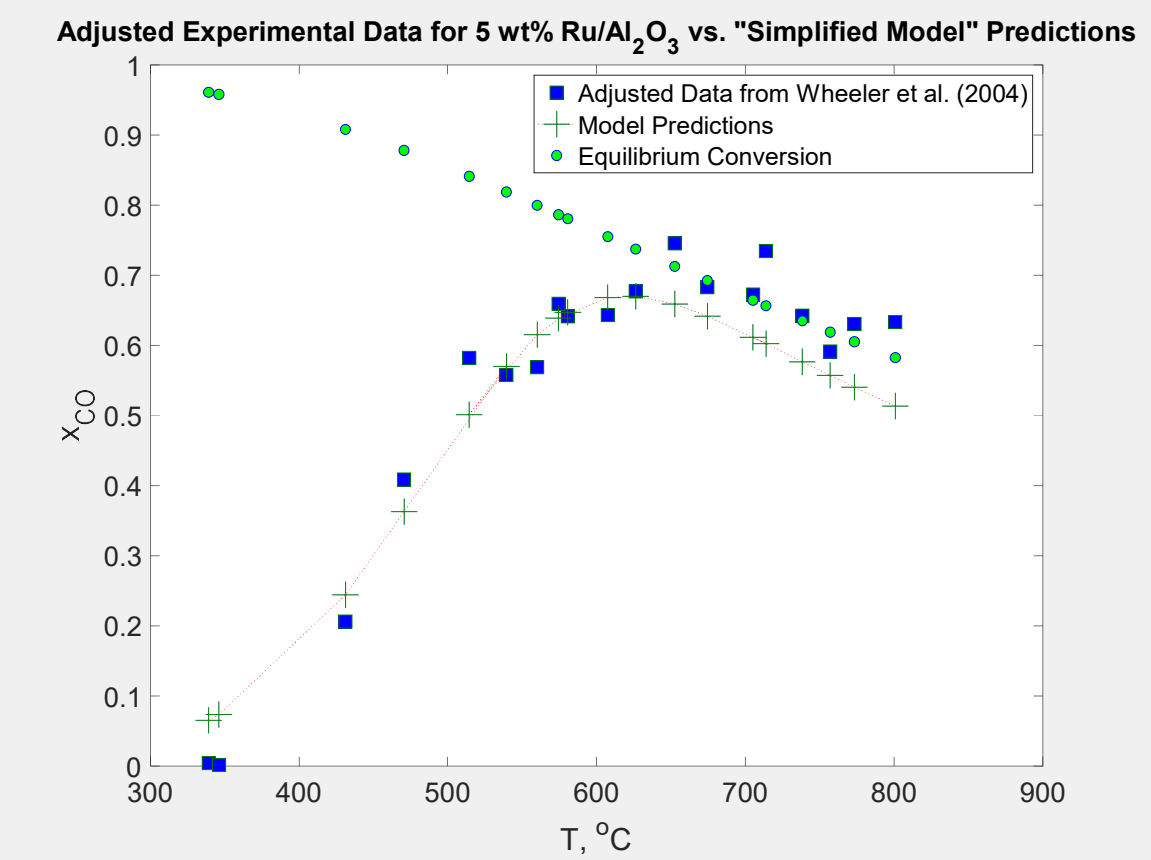

Figure 12: Predictions of the Simplified Model for the Conversion of Carbon Monoxide on a Ru/Al_2O_3 catalyst plotted against the (adjusted) experimental data collected by Wheeler et al.

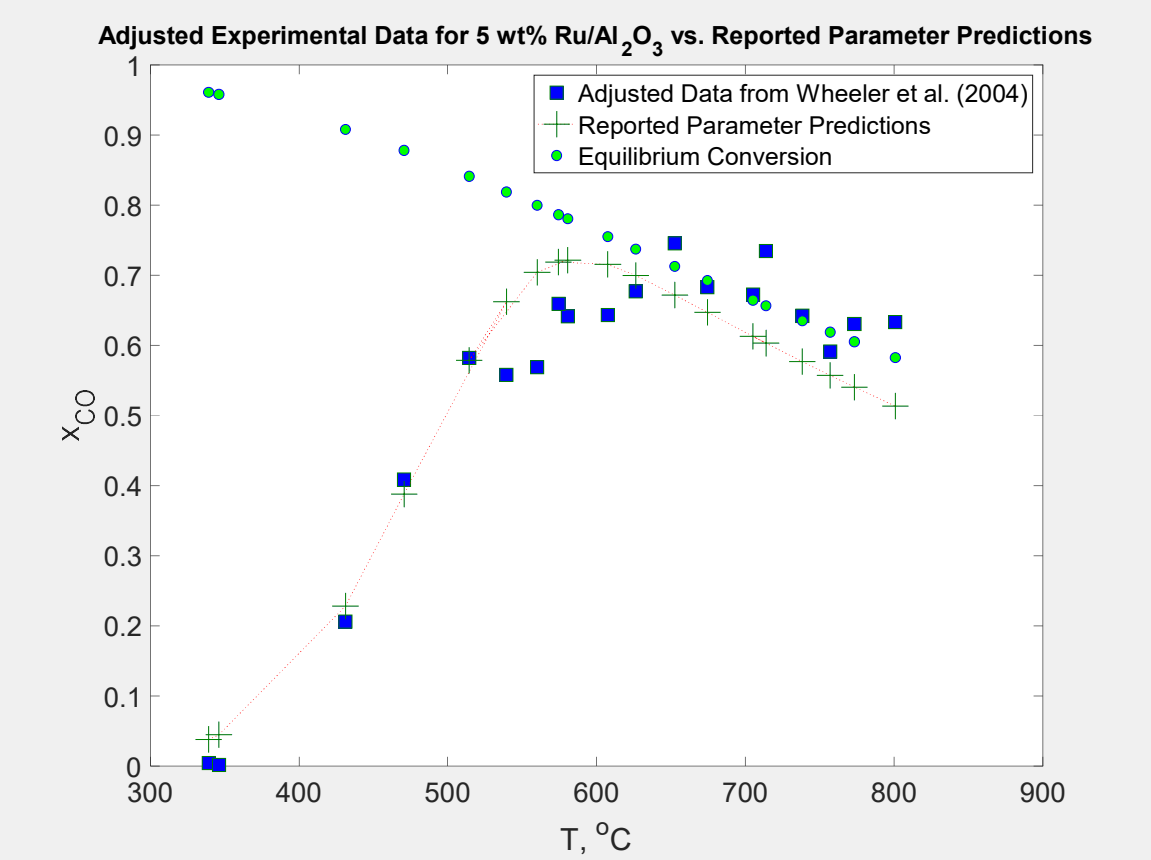

Figure 13: Predictions of the Simplified Model and the reported kinetic parameters for the Conversion of Carbon Monoxide on a Ru/Al_2O_3 catalyst plotted against the (adjusted) experimental data collected by Wheeler et al. (2004)

With both models predicting conversions below what is observed, it must be considered whether the assumption of constant hydrogen and water concentrations is the cause of this effect. The answer is no, for the experimental feed conditions did in fact result in relatively low changes in these components. Figure 14 shows the partial pressures of the reaction components along the length of the reactor for a single experiment at 626 ˚C. Table 8 quantifies the relative changes of the components.

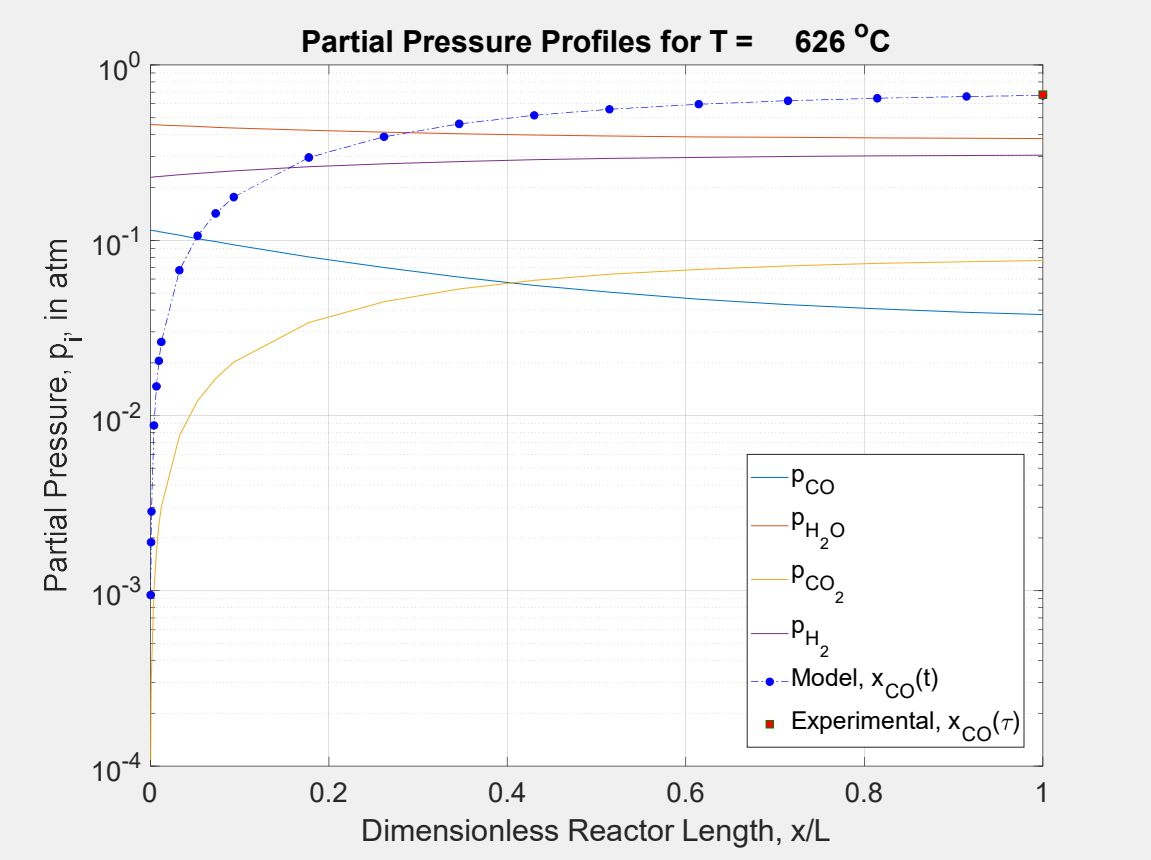

Figure 14: Partial Pressure Profiles along the dimensionless length of the Plug-Flow Reactor from which the experimental data was collected by Wheeler et al. [13] Temperature of the reactor is 626˚C and total pressure is 1 atm.

Components	CO	CO_2	H_2O	H_2
% Change	-76%	(Not in Feed)	-19%	+38%

Table 8: The compared changes of the components from the inlet of the tubular reactor catalyst bed to the outlet. These results were calculated from the data reported for a ruthenium-based catalyst experiment taking place at a temperature of 626 ˚C

This may suggest that the Simplified Model is applicable for conditions where water is in excess and hydrogen is included in the feed. This is particularly true in the region where conversion of carbon monoxide is not limited by equilibrium, where the agreement between model predictions and experimental data is within 19%. Once Equilibrium conditions are reached though, the model deviates significantly from the

experimental measurements. However, the fundamental shortcoming of this Simplified Model is that it cannot be applied to systems with different feed conditions than those used in the experiments to develop it. The results for the Excess Model (Table 9) will answer the question as to whether or not the predictions illustrated in Figure 12 and Figure 13 can be improved by a better interpretation of the α parameter in the *Simplified Model* as explained by Equation 18 & 28.

	Excess Model
$\overline{k}_{of}$	**2.0 ± 0.16** (s^{-1})
$\overline{E}_f$	**51.013 ± 0.005491** $\left(\frac{kJ}{mol}\right)$
$\overline{k}_{ob}$	**0.72 ± 0.06** (s^{-1})
$\overline{E}_b$	**88.04 ± 0.08802** $\left(\frac{kJ}{mol}\right)$

Table 9: Forward and backward reaction kinetic parameters for the water-gas shift reaction calculated using the Excess Model

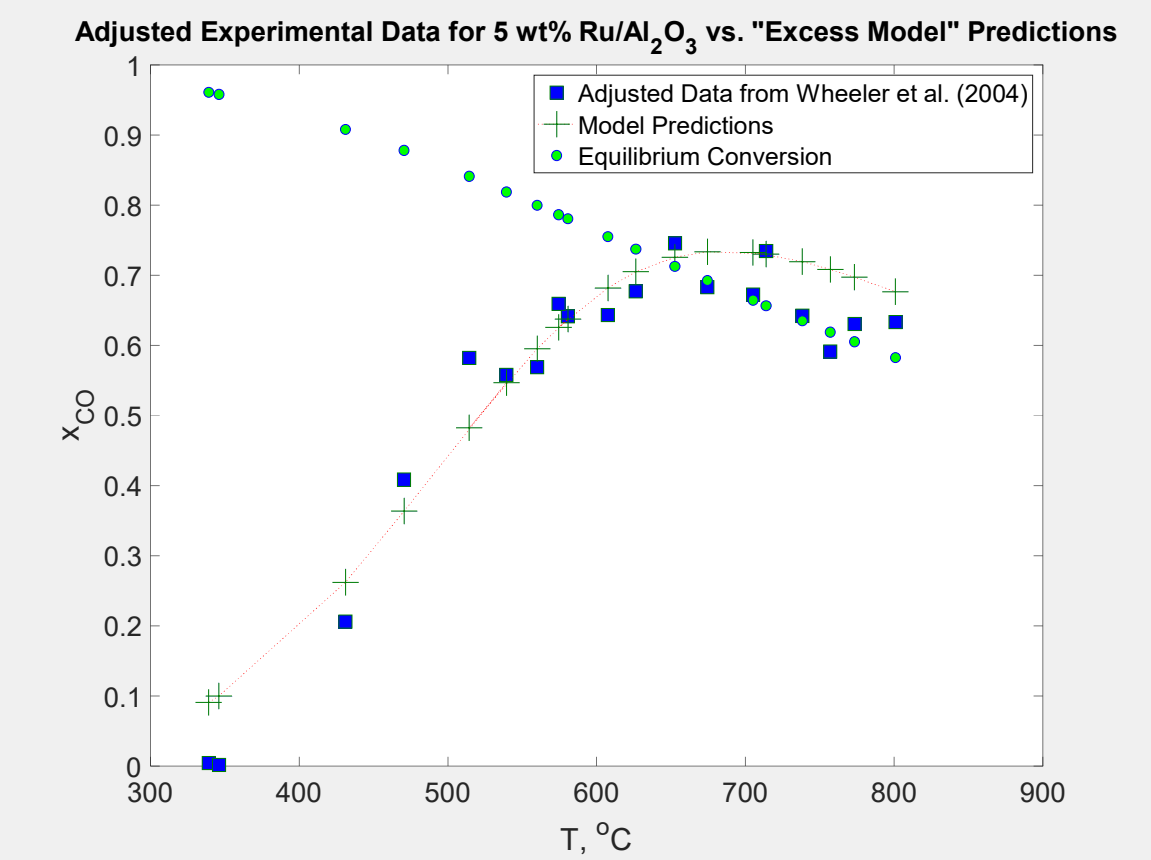

Figure 15: Predictions of the Excess Model for the Conversion of Carbon Monoxide on a Ru/Al_2O_3 catalyst plotted against the (adjusted) experimental data collected by Wheeler et al. [13]

Even while maintaining a consistent definition of K_c the *Excess Model* fails to accurately predict conversions of carbon monoxide at equilibrium conditions. This is similar to the shortcomings of the *Simplified Model*. However, the difference between the two is that the *Simplified Model* under-predicts carbon monoxide conversions at equilibrium and the *Excess Model* over-predicts these conversions. These results could've been anticipated by a close look at the derivations used to recover the models. The ratio of hydrogen to water in the feed is 0.5. When this factor is introduced in Equation 28 (where it is absent in Equation 18), the value of the α parameter increases and drives the conversion of carbon monoxide higher. Therefore, the correct introduction of the ratio of

the feed components in the *Excess Model* could've been predicted to increase the values of carbon monoxide conversion which is observed in the change from Figure 12 to Figure 15. The reason that neither model fits the data at equilibrium values is that the native backward reaction parameters cannot be recovered by the derivations of the *Simplified Model* or the *Excess Model.*

To recap, we proved that the assumption of constant values was valid for these experiments. This justified the use of the *Simplified Model*. Then, once the parameters reported by the paper could not be reproduced from the *Simplified Model*, the equation for α was adjusted to maintain a consistent definition of K_c that was lacking in the *Simplified Model.* The parameters from the paper could still not be reproduced. Thus, it was not the assumption of constant values or the inconsistent definition of K_c that was to blame for the poor predictions of the *Simplified Model* and the *Excess Model*. What complicates both models is the inability to retrieve the native rate constants or activation energies using a linear fit. Only pseudo-constants can be retrieved. We therefore suspect that a non-linear fitting method was used to recover the parameters reported by Wheeler et al. [13]. This would explain the absence of reported uncertainties. The *Bimolecular Model*, by contrast, can be used to retrieve the native kinetic parameters for the WGS with a linear fitting method.

The Bimolecular Model can be clearly seen to provide a better overall fit of the experimental data than its simplified counterparts (See Table 10). It is worth noticing that, although the calculations of the pre-exponential factors and activation energies excluded data points where conversion was affected by equilibrium, this model predicts equilibrium conversions to within 12%. While the fit is a major

improvement on that of the Simplified Model, the most important reason for this analysis is the need for a model and kinetic parameters that could be applied universally for the WGS regardless of feed conditions.

	Reported Parameters	*Simplified Model*	*Excess Model*	*Bimolecular Model*
R^2	**0.8854**	**0.9114**	**0.9241**	**0.9303**

Table 10: A summary of the coefficients of determination for each of the models analyzed in this paper. The Bimolecular Reaction Model accounts for the variation of all components of the reaction and provides better predictions of the conversion of carbon monoxide.

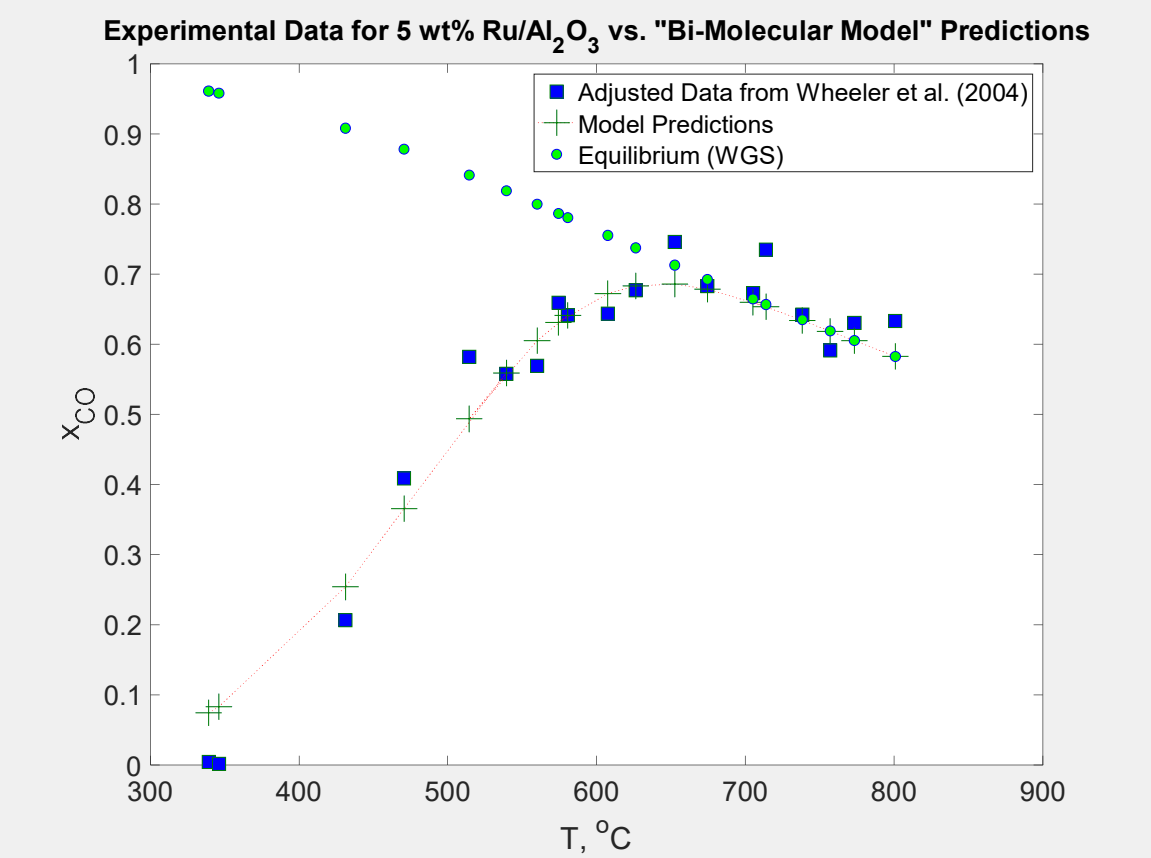

Figure 16: Predictions of the Bimolecular Reaction Model for the Conversion of Carbon Monoxide on a Ru/Al2O3¬ catalyst plotted against the Experimental Data collected by Wheeler et al. [13]

(at 5 wt%)	$k_{of}\left(\frac{L}{mol*s}\right)$	$E_f\left(\frac{kJ}{mol}\right)$	$k_{ob}\left(\frac{L}{mol*s}\right)$	$E_b\left(\frac{kJ}{mol}\right)$
Pt/Al_2O_3	$6.007 \times 10^8 \pm 3.1 \times 10^8$	93.37 ± 0.003733	$3.601 \times 10^{10} \pm 1.9 \times 10^{10}$	130.40 ± 0.1304
Ru/Al_2O_3	380 ± 32	64.24 ± 0.005316	140 ± 11	101.27 ± 0.1013

Table 11: Kinetic parameters for the forward water-gas shift reaction on noble metal-based catalysts of interest to waste gasification

Percent Gasification and Product Compositions Trends

The final percent gasification values shown below were calculated from the averages of the molar compositions for the produced carbonaceous gases after the outlier analysis discussed in Chapter III was performed. For all compositions and gasification percentages, the uncertainty in the reaction time is assumed to be no more than 0.3 hours. This value is considered a conservative estimate. In the experiments the reaction quenching was initiated at the times shown by shutting down the heating and initiating rapid cooling. This protocol, coupled with the ramping technique used to bring the reactor to the reaction temperature under analysis, was considered reliable so as to identify reaction times. Since both heating and quenching stages exhibit short dynamics, 0.3 hours is considered to provide a conservative window for data presentation.

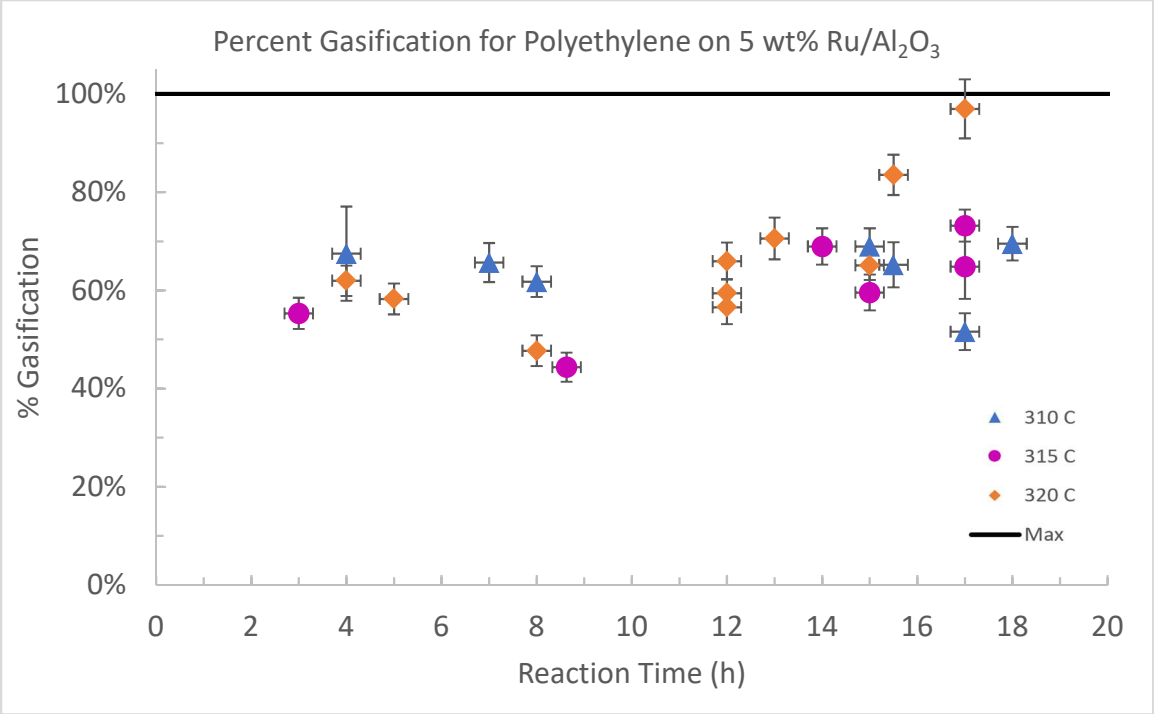

Figure 17: Percent gasification data obtained from thermodynamic data on reactor and GC data for carbonaceous gas compositions.

The most obvious trend in the data is that the % Gasification will typically increase with reaction time. This is because the % Gasification is defined in terms of the loading of substrate and since the oxidation reactions which destroy the substrate are irreversible, longer reactions will typically mean more oxidation of the polymer. Since these gas-phase reactions are the mechanisms for turning the carbon monoxide and carbon dioxide products into higher value products (i.e. methane and hydrogen), higher percent gasification may not correlate well with efficiency of gasification. We can see in the data presented here that higher percent gasification can attribute its magnitude to the composition of carbon dioxide in the product gas rather than methane.

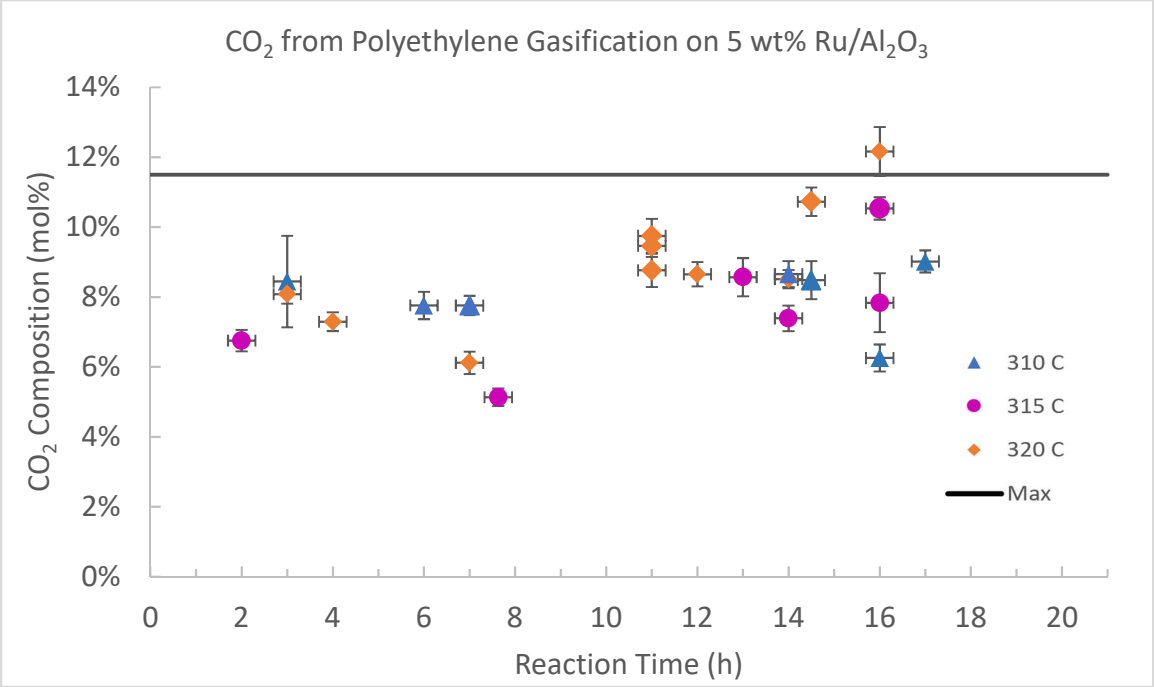

Figure 18: Compositions of CO_2 in product gas for polyethylene batch reactions. Black line indicates maximum possible CO_2 composition for an ideal reaction under the given conditions. Data was obtained by GC-TCD.

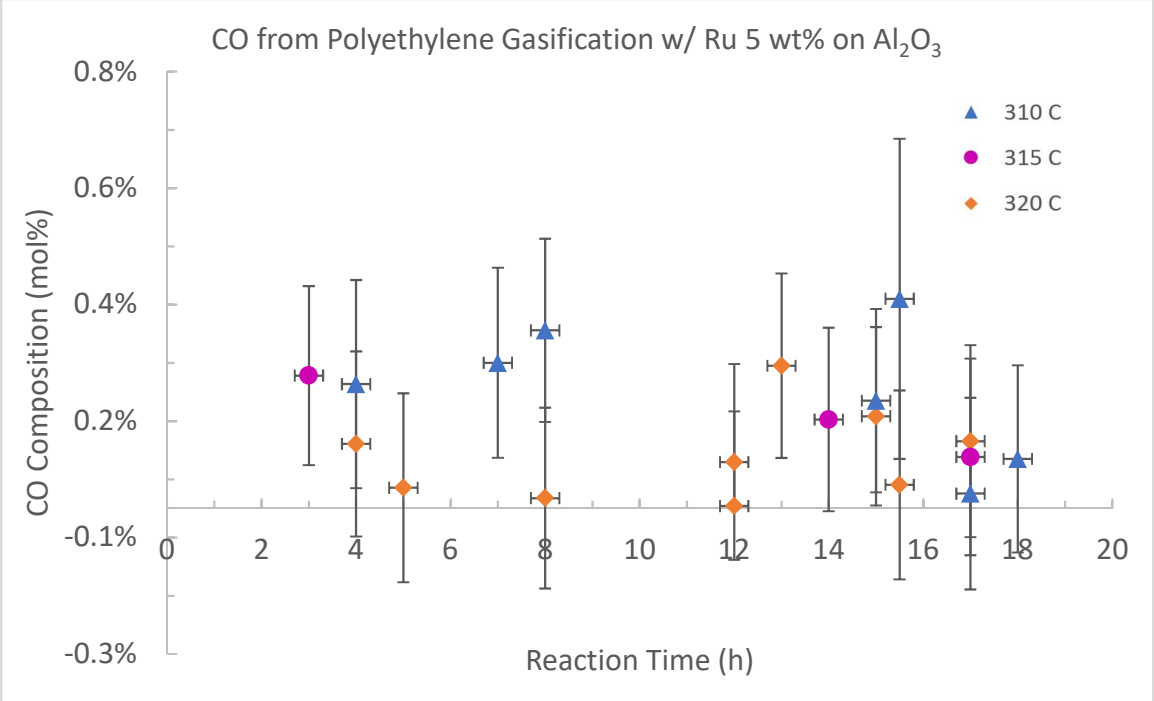

Figure 19: Compositions of CO in product gas for polyethylene batch reactions. Data was obtained by GC-TCD.

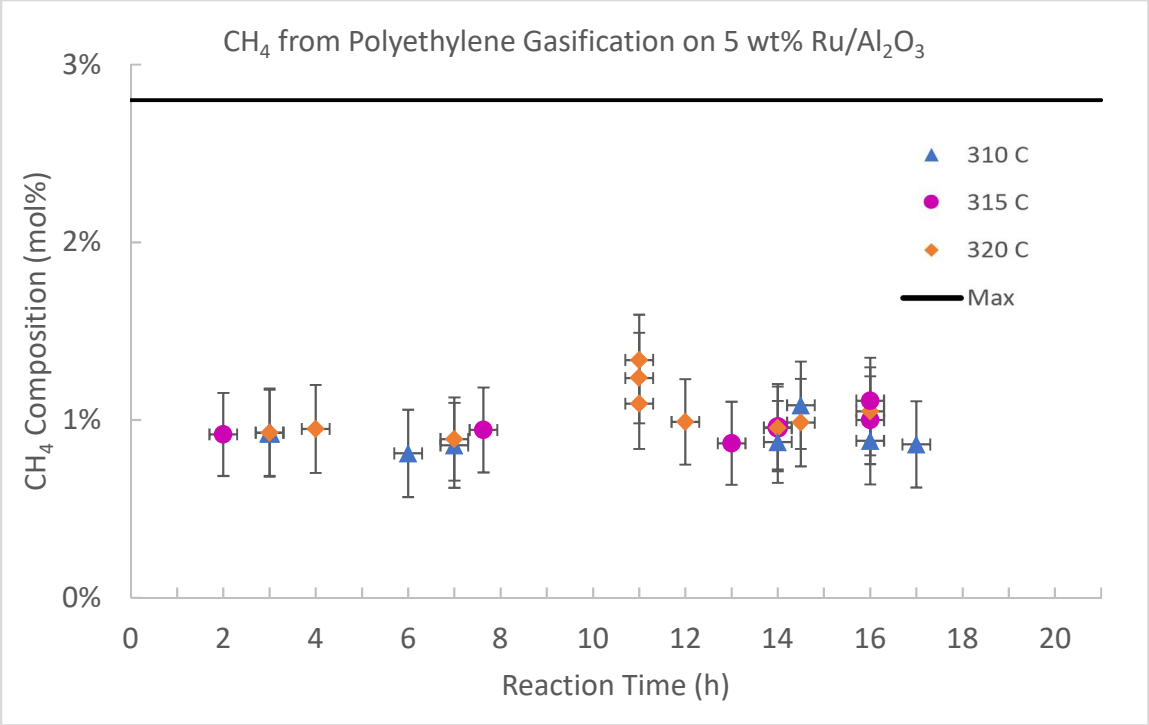

Figure 20: Compositions of CH_4 in product gas for polyethylene batch reactions. Black line indicates maximum possible CH4 composition for an ideal reaction under the given conditions. Data was obtained by GC-TCD.

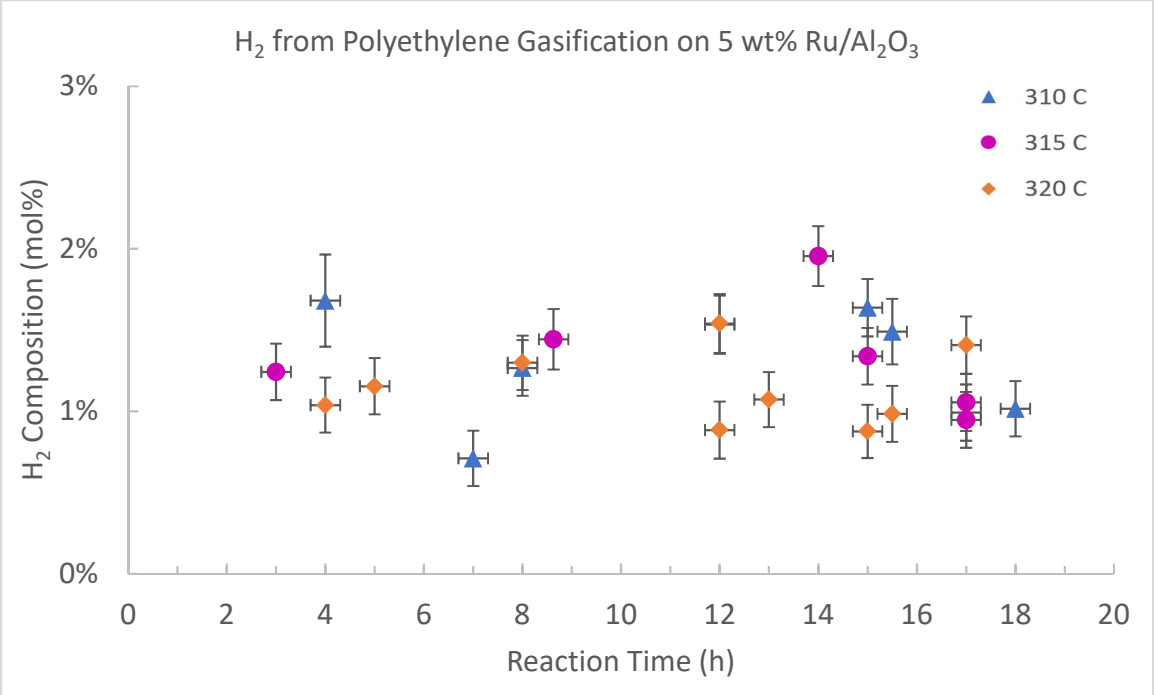

Figure 21: Compositions of H_2 in product gas for polyethylene batch reactions. Data was obtained by GC-TCD.

Looking at results for carbon monoxide (Figure 19), concentrations are consistently low for all temperatures investigated. This may indicate that the water-gas shift reaction is converting most of the carbon monoxide produced. If there were no methane present in the product gas, then it would indicate that the oxidation phase is heavily favoring the pathway to carbon dioxide over the pathway to carbon monoxide. However, as can be seen in Figure 20, this is not the case for methane is appearing in the syngas.

The reaction time and studied temperatures have little effect on the methane composition but appear to, by comparison, more significantly impact the concentration of hydrogen. The relative consistency in methane composition indicates that the Sabatier reaction is reaching equilibrium. Hydrogen produced and consumed by the water-gas shift and Sabatier reactions respectively and is not expected to continually increase but experience a peak composition. This is in contrast to carbon dioxide which can be expected to continually increase due to its production in two of the four major reactions and the limitation on its consumption in the Sabatier made apparent by the results for methane. The fluctuation in the composition of hydrogen observed in the data may indicate that the process can be further optimized to produce more carbon monoxide for the water-gas shift reaction.

The observations in the GC data are all in agreement with the knowledge that water is in high excess in the gas-phase at the temperatures investigate. Table 12 shows the saturation pressures and molar counts (calculated by the Ideal Gas Law) during the reactions. With only 0.0021 moles of polyethylene monomer loaded in each experiment, the amount of water can be relied upon to exceed the amounts of any of the syngas

components by orders of magnitude. This would drive the water-gas shift to significant conversion of carbon monoxide and put a hard cap on the forward Sabatier reaction.

T (˚C)	P^{sat} (psia)	P^{tot} (psia)	$n_{H_2O,vap}$ (mol)
310	1447.52	1530	0.1646
315	1548.14	1636	0.1746
320	1653.80	1740	0.1849

Table 12: Amount of water in the gas-phase at the reaction temperatures investigated.

A clear extension to this analysis can be completed using equilibrium thermodynamics for the gas-phase reactions to calculate hydrogen compositions, which would provide additional validation to the GC analysis. Carbon dioxide and methane are the most reliable points in the GC analysis and the equilibrium data and saturation pressures of water are readily available. This verification will be helpful because hydrogen possesses the highest errors in the calibration curve when compared to the other components and does not reveal obvious trends in the GC data.

Selectivity of Oxidation

Although there is much to learn qualitatively from the composition data previously discussed, more can be understood quantitatively by analyzing the selectivities of the syngas components. If we want to optimize the process to produce more carbon dioxide for the water-gas shift reaction, then an understanding of how the oxidation reactions compete is essential.

Difficulties in the measurement of carbon monoxide were found and had been expected. Although information on the abundance of water in the experiments justifies a hypothesis of total consumption of carbon monoxide by the water-gas shift reaction,

values recorded via GC analysis often reached not just low but negative values. Despite efforts to limit silica gel adsorption of carbon monoxide in the sample cylinders, this potential for interaction with the sample gas presents uncertainty in carbon monoxide data. Additionally, the carbon monoxide peak in the chromatograms is significantly shouldering the nitrogen peak which is massive. Thus, a handful of data points for the selectivity of carbon monoxide proved useless in the analysis of the selectivity of oxidation. This limited the data set.

After removal of obvious outliers and obsolete data points, it is then necessary to smooth out the data to avoid error introduced by differentiation. The interpolated points are differentiated and Equations 49 and 50 are solved for all reaction times to find the reaction rates.

Temperature (˚C)	$\frac{k_1}{k_2}$
310	2.0601
320	0.49 ± 0.016

Table 13: Ratios of polyethylene oxidation over a 5 wt% Ru/Al_2O_3 catalyst at different reaction temperatures.

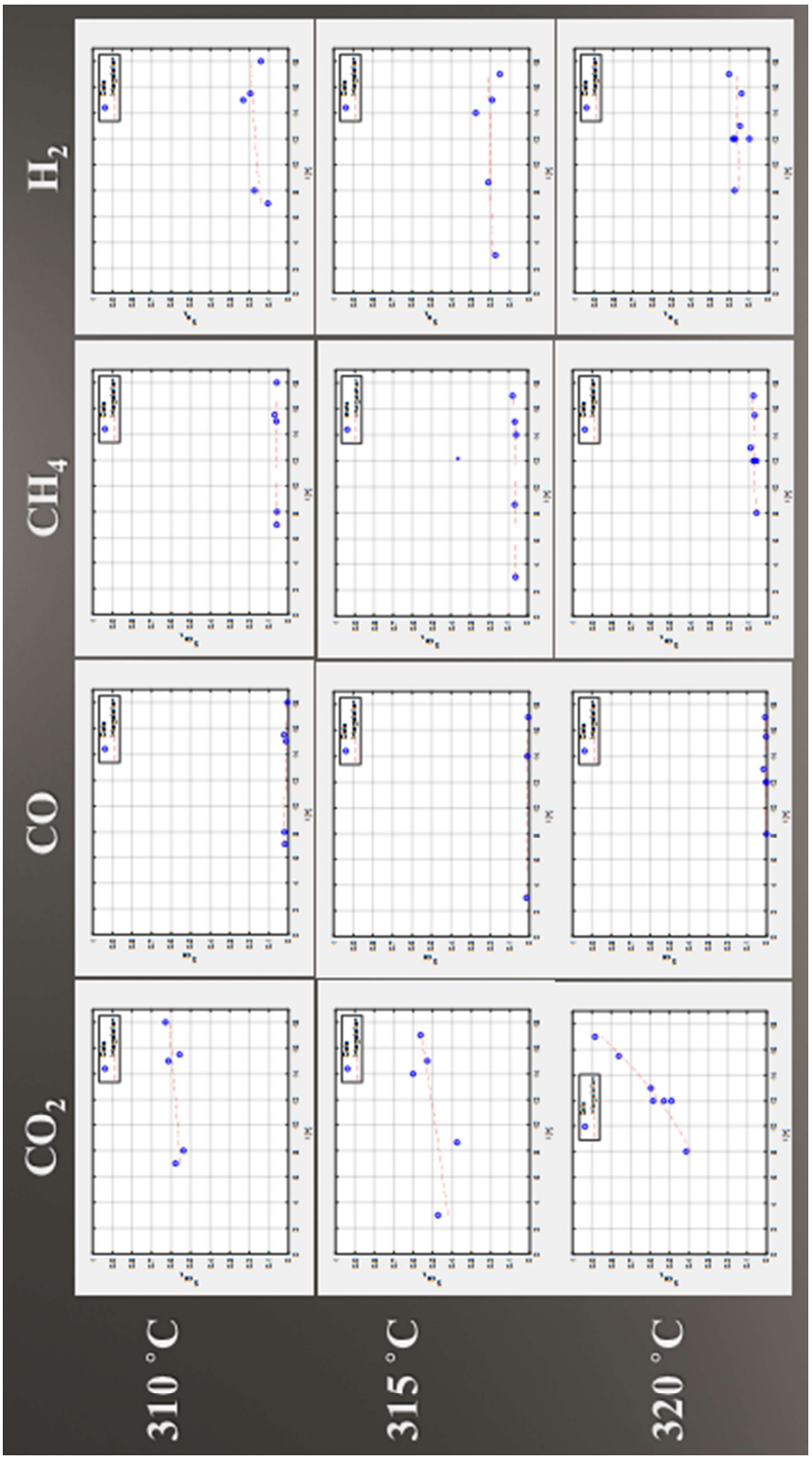

Figure 22: Selectivities of components analyzed plotted with their trends. For 315 ℃ there are only 3 useful data points for carbon monoxide. This greatly limits the ability to draw conclusions.

When a constant ratio of the reaction rates with respect to reaction temperature was not observed, the results indicated a difference in the orders of the reactions with respect to polyethylene monomer.

Temperature (˚C)	$n_1 - n_2$
310	0
320	-3.11 ± 0.0524

Table 14: Difference in the order of reaction for the carbon dioxide and carbon monoxide oxidation reactions in a polyethylene gasification process over a 5 wt% Ru/Al_2O_3 catalyst.

CHAPTER V

CONCLUSIONS & RECOMMENDATIONS

The kinetic parameters for the water-gas shift reaction were recovered with reportable uncertainty to be applied to waste gasification for platinum and ruthenium catalysts supported by alumina. In succession to a previous study recovering the kinetic parameters for the Sabatier reaction [8], this marks the completion of the kinetic studies on the gas-phase reactions. Now, the parameters for both of these reactions can be applied to gasification experiments and processes for any substrate.

Gasification was observed in all experiments on polyethylene over a 5 wt% Ru/Al_2O_3 catalyst. Methane was proven to be reaching equilibrium concentrations beyond 3 hours of reaction and 310 ˚C within the data set. The fluctuation and relative magnitude of hydrogen measured indicated the potential for further optimization of the oxidation phase to produce more carbon monoxide for the water-gas shift reaction. A method of analysis was derived to recover the selectivity of oxidation for polyethylene and preliminary results were reported to indicate a potential relationship between the selectivity of oxidation and temperature where the carbon monoxide production rate approaches that of carbon dioxide as temperature increases.

Conflicting implications are observed by the differences in the orders of reaction for 310 and 320 ˚C. Both temperatures should report the same difference as the order of reaction is not dependent on conversion or temperature. We learned that shorter reaction times should be investigated to recover the oxidation kinetics if a difference in the orders of reaction proves to be greater than zero. The data set for 315 ˚C proved to be too small to draw quantitative conclusions regarding the selectivity of oxidation or reaction kinetics but helped to further reinforce the observations that methane is reaching equilibrium limitations.

In the future, we would like to collect GC data for shorter reaction times at more temperatures up to 350 ˚C. We would also like to gather data for a similar range of reaction times at 310 ˚C using platinum catalyst at 5 wt% on alumina and observe the effect on the selectivity of oxidation. If an improvement is observed (a decrease in the ratio), then a combination of a platinum and ruthenium catalyst at an unknown ratio may be the optimal catalyst for waste gasification of polyethylene.

REFERENCES

1. Atassi, L., *From waste to watts: Cleveland's controversial pursuit of trash conversion technology*, in *The Plain Dealer*2012.
2. Jarboe-McFee, M., *With waste-to-energy project, Forest City and Quasar Energy Group chart renewable course*, in *The Plain Dealer*2012.
3. Hepp, A.F., et al., *Green Aerospace Fuels Non-petroleum Sources*, 2011.
4. Kulis, M.J., et al., *Development of a Catalytic Wet Air Oxidation Method to Produce Feedstock gases from Waste Simulant*, in *44th Inernat. Conf. on Environ. Systems (ICES)*2014: Tucson, AZ.
5. Al-Salem, S.M., P. Lettieri, and J. Baeyens, *Recycling and recovery routes of plastic solid waste (PSW): A review.* Waste Management, 2009. **29**(10): p. 2625-2643.
6. Santiago-Maldonado, E., et al., *Creating Methane from Plastic: Recycling at a Lunar Outpost* in *48th AIAA Aerospace Sciences Meeting*2010: Orlando, FL.
7. Lunde, P.K., FL, *Carbon Dioxide Methanation on a Ruthenium Catalyst. Industrial & Engineering Chemistry Process Design and Development*, 1974. **13**(1): p. 27-33.
8. Lange, E., DeMattia, B. & Gatica, J., *Catalytic Gasification - A Critical Analysis of Carbon Dioxide Methanation on a Ru/Al_2O_3 Catalyst.* International Journal of Chemical Reactor Engineering, 2018. **16**(7).
9. Smith, B.M., L & Murthy, Loganathan & Shantha, Shekhar. , *A Review of the Water Gas Shift Reaction Kinetics.* International Journal of Chemical Reactor Engineering, 2010. **8**(1).

10. Grenoble, D.C., M.M. Estadt, and D.F. Ollis, *The chemistry and catalysis of the water gas shift reaction: 1. The kinetics over supported metal catalysts.* Journal of Catalysis, 1981. **67**(1): p. 90-102.

11. Utaka, T., et al., *Water gas shift reaction of reformed fuel over supported Ru catalysts.* Applied Catalysis A: General, 2003. **245**(2): p. 343-351.

12. Panagiotopoulou, P. and D.I. Kondarides, *Effect of the nature of the support on the catalytic performance of noble metal catalysts for the water–gas shift reaction.* Catalysis Today, 2006. **112**(1): p. 49-52.

13. Wheeler, C., et al., *The water–gas-shift reaction at short contact times.* Journal of Catalysis, 2004. **223**(1): p. 191-199.

14. Choi, Y. and H.G. Stenger, *Water gas shift reaction kinetics and reactor modeling for fuel cell grade hydrogen.* Journal of Power Sources, 2003. **124**(2): p. 432-439.

15. EPA, *Municipal Solid Waste*, E.P. Agency, Editor 2013.

16. Al-Salem, S.M., P. Lettieri, and J. Baeyens, *Recycling and recovery routes of plastic solid waste (PSW): A review.* Waste Management, 2009. **29**(10): p. 2625-2643.

17. Stanley, D., *NASA's Exploration Systems Architecture Study*, 2005: Washington, D.C. NASA Headquarters.

18. Panda, A.K., R.K. Singh, and D.K. Mishra, *Thermolysis of waste plastics to liquid fuel: A suitable method for plastic waste management and manufacture of value added products—A world prospective.* Renewable and Sustainable Energy Reviews, 2010. **14**(1): p. 233-248.

19. Bunluesin, T. and R.J. Gorte, *Studies of the water-gas-shift reaction on ceria-supported Pt, Pd, and Rh: implications for oxygen-storage properties.* Applied Catalysis B: Environmental, 1998. **15**(1-2): p. 107-114.

20. Hilaire, S., et al., *A comparative study of water-gas-shift reaction over ceria supported metallic catalysts.* Applied Catalysis A: General, 2001. **215**: p. 271.

21. Wang, X. and R.J. Gorte, *The effect of Fe and other promoters on the activity of Pd/ceria for the water-gas shift reaction.* Applied Catalysis A: General, 2003. **247**(1): p. 157-162.

22. Shido, T. and Y. Iwasawa, *Reactant-Promoted Reaction Mechanism for Water-Gas Shift Reaction on Rh-Doped CeO2.* Journal of Catalysis, 1993. **141**(1): p. 71-81.

APPENDIX A: NOMENCLATURE

Water-Gas Shift Analysis		
Symbol	Values/(Units)	Description
r_{CO}^{w}	$\left(\frac{pressure}{vol * time}\right)$	Reaction rate of carbon monoxide in the water-gas shift reaction as described by Wheeler et al. (2004)
r_{CO}	$\left(\frac{mol}{L * s}\right)$	Reaction rate of carbon monoxide in the water-gas shift reaction in this paper's analysis
k_f^w	$(?)$	Forward rate constant for the water-gas shift reaction as described by Wheeler et al. (2004)
k_b^w	$(?)$	Backward rate constant for the water-gas shift reaction as described by Wheeler et al. (2004)
$\overline{k_f}$	(s^{-1})	Forward pseudo-constant for the water-gas shift
$\overline{k_b}$	(s^{-1})	Backward pseudo-constant for the water-gas shift
$\overline{k_o}$	(s^{-1})	
k_f	$\left(\frac{L}{mol * s}\right)$	Forward rate constant for the water-gas shift reaction in this paper's analysis
k_b	$\left(\frac{L}{mol * s}\right)$	Backward rate constant for the water-gas shift reaction in this paper's analysis
k_o	$\left(\frac{L}{mol * s}\right)$	
A_f	$\left(\frac{L}{mol * s}\right)$	Forward pre-exponential factor for the water-gas shift reaction
$\overline{A_f}$	(s^{-1})	Forward pseudo-pre-exponential factor for the water-gas shift reaction
A_b	$\left(\frac{L}{mol * s}\right)$	Backward pre-exponential factor for the water-gas shift reaction
$\overline{A_b}$	(s^{-1})	Backward pseudo-pre-exponential factor for the water-gas shift reaction
ΔH_R	$\left(\frac{kJ}{mol}\right)$	Enthalpy of reaction
E_f	$\left(\frac{kJ}{mol}\right)$	Forward reaction activation energy
$\overline{E_f}$		Forward reaction pseudo-activation energy
E_b	$\left(\frac{kJ}{mol}\right)$	Backward reaction activation energy
$\overline{E_b}$		Backward reaction pseudo-activation energy
P_{CO}	$(pressure)$	Partial pressure of carbon monoxide
P_{H_2O}	$(pressure)$	Partial pressure of water
P_{CO_2}	$(pressure)$	Partial pressure of carbon dioxide
P_{H_2}	$(pressure)$	Partial pressure of hydrogen
C_{CO}	$\left(\frac{mol}{L}\right)$	Concentration of carbon monoxide at reactor outlet
C_{H_2O}	$\left(\frac{mol}{L}\right)$	Concentration of water at reactor outlet

C_{CO_2}	$\left(\frac{mol}{L}\right)$	Concentration of carbon dioxide at reactor outlet
C_{H_2}	$\left(\frac{mol}{L}\right)$	Concentration of hydrogen at reactor outlet
C_{CH_4}	$\left(\frac{mol}{L}\right)$	Concentration of methane at reactor outlet
C_{CO}^{in}	$\left(\frac{mol}{L}\right)$	Concentration of carbon monoxide at reactor inlet
$C_{H_2O}^{in}$	$\left(\frac{mol}{L}\right)$	Concentration of water at reactor inlet
$C_{H_2}^{in}$	$\left(\frac{mol}{L}\right)$	Concentration of hydrogen at reactor inlet
a	$\left(\frac{mol}{L}\right)$	Coefficient of second order term in quadratic formula
b	$\left(\frac{mol}{L}\right)$	Coefficient of first order term in quadratic formula
c	$\left(\frac{mol}{L}\right)$	Coefficient of zeroth order term in quadratic formula
q	Dimensionless	First root of quadratic
p	Dimensionless	Second root of quadratic
F_{CO}	$\left(\frac{mol}{s}\right)$	Molar flow rate of carbon monoxide at the reactor outlet
θ_B	Dimensionless	Feed ratio of water to carbon monoxide
θ_C	Dimensionless	Feed ratio of carbon dioxide to carbon monoxide
θ_D	Dimensionless	Feed ratio of hydrogen to carbon monoxide
$X_{CO,T}$	Dimensionless	Total conversion of carbon monoxide. Corresponds to conversions of carbon monoxide reported by Wheeler et al. (2004).
$X_{CO,1}$	Dimensionless	Adjusted conversion of carbon monoxide. Corresponds to conversions of carbon monoxide as a result of only the water-gas shift.
$X_{CO,1}^{Exp}$	Dimensionless	Experimental adjusted conversion of carbon monoxide. Corresponds to conversions of carbon monoxide as a result of only the water-gas shift.
$X_{CO,1}^{pred}$	Dimensionless	Predicted adjusted conversions of carbon monoxide. Corresponds to conversions of carbon monoxide as a result of only the water-gas shift.
$\overline{X}_{CO,1}^{pred}$	Dimensionless	Mean of the predicted adjusted conversions of carbon monoxide. Corresponds to conversions of carbon monoxide as a result of only the water-gas shift.
$X_{CO,2}$	Dimensionless	Conversion of carbon monoxide due to the Sabatier reaction
S_{CH_4}	Dimensionless	Selectivity of methane in the experiments of Wheeler et al. (2004) defined in terms of carbon monoxide converted.

K_c	Dimensionless	Concentration equilibrium constant
K_o		
α	Dimensionless	Alpha factor for derivation
ε	0.80	Void fraction of reactor catalyst bed
R	$0.008314\ \frac{kJ}{K*mol}$	Universal gas constant
T	(K)	Reaction temperature
T^{ref}	$873.15\ K$	Reference temperature
T^o	298.15 K	Standard conditions temperature
V	(L)	Packed bed reactor volume
Q^o	$3\ SLPM$	Inlet volumetric flow rate in standard liters per minute
t	(s)	Time of reaction
τ	(s)	Reactor residence time
RSS	Dimensionless	Sum of squared residuals
TSS	Dimensionless	Total sum of squares
R^2	Dimensionless	Coefficient of determination

Selectivity of Oxidation Analysis		
Symbol	Values/(Units)	Description
S_i	Dimensionless	Selectivity of component i
S_A	Dimensionless	Selectivity of polyethylene (PE)
S_D	Dimensionless	Selectivity of desired product
S_U	Dimensionless	Selectivity of undesired product
S_{CO}	Dimensionless	Selectivity of carbon monoxide
S_{CO_2}	Dimensionless	Selectivity of carbon dioxide
S_{CH_4}	Dimensionless	Selectivity of methane
S_{H_2}	Dimensionless	Selectivity of hydrogen
S_{co/co_2}	Dimensionless	Selectivity of oxidation
X_A	Dimensionless	Conversion of polyethylene
r_1	$\left(\frac{mol}{L*h}\right)$	Reaction rate of polyethylene to carbon dioxide oxidation reaction
r_2	$\left(\frac{mol}{L*h}\right)$	Reaction rate of polyethylene to carbon monoxide oxidation reaction
r_3	$\left(\frac{mol}{L*h}\right)$	Reaction rate of water-gas shift reaction
r_4	$\left(\frac{mol}{L*h}\right)$	Reaction rate of Sabatier reaction
r_{co}	$\left(\frac{mol}{L*h}\right)$	Reaction rate of polyethylene to carbon monoxide oxidation reaction with respect to carbon monoxide
r_{co_2}	$\left(\frac{mol}{L*h}\right)$	Reaction rate of polyethylene to carbon dioxide oxidation reaction with respect to carbon dioxide
r_A	$\left(\frac{mol}{L*h}\right)$	Reaction rate of polyethylene to carbon dioxide oxidation reaction with respect to polyethylene

k_1	(h^{-1})	Rate constant for the polyethylene to carbon dioxide oxidation reaction
k_2	(h^{-1})	Rate constant for the polyethylene to carbon monoxide oxidation reaction
$k_{1/2}$	(h^{-1})	Placeholder for either k_1 or k_2
n	Dimensionless	Order of reaction
C_A	$\left(\frac{mol}{L}\right)$	Concentration of polyethylene monomer in the liquid phase
N_i	(mol)	Moles of component i at end of reaction
N_A^o	(mol)	Initial moles of polyethylene monomer (C_2H_4)
V_1	20 mL	Volume of the liquid phase in wet thermal catalytic gasification (approximate)
V_2	80 mL	Volume of the gas phase in wet thermal catalytic gasification (approximate)
t	(h)	Reaction time

Chapter III Nomenclature		
Symbol	Values/(Units)	Description
X_{sub}	Dimensionless	Percent Gasifcation (Equivalent to conversion of PE)
$X_{C_2H_4}$	Dimensionless	Percent Gasifcation (Equivalent to conversion of PE)
X_{CO}	Dimensionless	Conversion of carbon monoxide in the water-gas shift
X_{H_2}	Dimensionless	Conversion of hydrogen in the Sabatier reaction
$n_{C,prod}$	(mol)	Moles of carbon produced
$n_{C,loaded}$	(mol)	Moles of carbon loaded
c	Dimensionless	Number of carbons in monomer
$n_{monomer}$	(mol)	Moles of monomer
P^{col}	$(psia)$	Pressure of the reactor vessel immediately before collecting sample
P^{cyl}	$(psig)$	Pressure of the sample cylinder
P^{sam}	$(psig)$	Partial pressure of the sample gas loaded into the sample cylinder
P^{He}	$(psig)$	Partial pressure of the helium gas loaded into the sample cylinder
V_{cyl}	(mL)	Volume of the sample cylinder
T^{cyl}	(K)	Temperature of the sample cylinder (Assumed to be 298.15 K)
T^{col}	(K)	Temperature of the reactor vessel immediately before collecting sample
y_i	$(mol\%)$	Molar composition of component *i*
m_i	$\left(\frac{mol}{area}\right)$	Slope of the calibration curve for component *i*
x_i	$(area)$	Average area count of injections for component *i*
σ_i	$(area)$	Standard error of area counts for component *i*
n	Dimensionless	Number of injections

b_i	$(mol\%)$	Intercept of the calibration curve for component *i*
y_{CO}	$(mol\%)$	Molar composition of carbon monoxide
y_{CO_2}	$(mol\%)$	Molar composition of carbon dioxide
y_{CH_4}	$(mol\%)$	Molar composition of methane
n_{sam}	(mol)	Moles of the sample gas loaded into the sample cylinder
n_{He}	(mol)	Moles of the helium gas loaded into the sample cylinder
n_{tot}	(mol)	Total moles of gas in the sample cylinder
$n_{CO_2,1}$	(mol)	Moles of carbon dioxide produced in the oxidation phase
$n_{CO_2,2}$	(mol)	Moles of carbon dioxide after the water-gas shift
$n_{CO,1}$	(mol)	Moles of carbon monoxide produced in the oxidation phase
n_{O_2}	(mol)	Moles of oxygen loaded
$n_{O_2,1}$	(mol)	Moles of oxygen remaining after the oxidation phase
$n_{H_2,2}$	(mol)	Moles of hydrogen produced by the water-gas shift
n_{CH_4}	(mol)	Moles of methane produced by the Sabatier reaction
n_{PE}	(mol)	Moles of polyethylene
z		Oxidation fraction to carbon dioxide
m_A	(g)	Mass of substrate
M_A	$\left(\frac{g}{mol}\right)$	Molar mass of substrate monomer

APPENDIX B: CORRELATION OF K_c

T^o	600	873.15
T	$1/T - 1/T^o$	ln(Keq)
K	K^{-1}	[dim]
573.15	0.000599	3.720674
578.15	0.000584	3.649772
583.15	0.00057	3.580172
588.15	0.000555	3.511841
593.15	0.000541	3.444745
598.15	0.000527	3.37885
603.15	0.000513	3.314131
608.15	0.000499	3.250557
613.15	0.000486	3.188095
618.15	0.000472	3.126725
623.15	0.000459	3.066414
628.15	0.000447	3.007137
633.15	0.000434	2.948871
638.15	0.000422	2.891593
643.15	0.00041	2.835276
648.15	0.000398	2.779899
653.15	0.000386	2.725445
658.15	0.000374	2.671884
663.15	0.000363	2.619197
668.15	0.000351	2.56737
673.15	0.00034	2.516373
678.15	0.000329	2.466199
683.15	0.000319	2.416824
688.15	0.000308	2.368223
693.15	0.000297	2.320396
698.15	0.000287	2.273313
703.15	0.000277	2.22696
708.15	0.000267	2.181322
713.15	0.000257	2.136384
718.15	0.000247	2.092131
723.15	0.000238	2.048547
728.15	0.000228	2.00562
733.15	0.000219	1.963335
738.15	0.000209	1.921677
743.15	0.0002	1.880637
748.15	0.000191	1.840199
753.15	0.000182	1.800352

758.15	0.000174	1.761084
763.15	0.000165	1.722381
768.15	0.000157	1.684236
773.15	0.000148	1.646633
778.15	0.00014	1.609566
783.15	0.000132	1.573023
788.15	0.000124	1.53699
793.15	0.000116	1.501461
798.15	0.000108	1.466426
803.15	9.98E-05	1.431875
808.15	9.21E-05	1.397795
813.15	8.45E-05	1.364184
818.15	7.7E-05	1.33103
823.15	6.96E-05	1.298321
828.15	6.22E-05	1.266054
833.15	5.5E-05	1.234215
838.15	4.78E-05	1.202804
843.15	4.07E-05	1.171804
848.15	3.38E-05	1.141215
853.15	2.68E-05	1.111025
858.15	2E-05	1.081232
863.15	1.33E-05	1.051821
868.15	6.6E-06	1.022789
873.15	0	0.994133
878.15	-6.5E-06	0.965843
883.15	-1.3E-05	0.937907
888.15	-1.9E-05	0.910329
893.15	-2.6E-05	0.883098
898.15	-3.2E-05	0.856205
903.15	-3.8E-05	0.829652
908.15	-4.4E-05	0.803427
913.15	-5E-05	0.77752
918.15	-5.6E-05	0.75194
923.15	-6.2E-05	0.726664
928.15	-6.8E-05	0.7017
933.15	-7.4E-05	0.677043
938.15	-7.9E-05	0.652679
943.15	-8.5E-05	0.628603
948.15	-9.1E-05	0.604819
953.15	-9.6E-05	0.581321
958.15	-0.0001	0.558095

963.15	-0.00011	0.535147
968.15	-0.00011	0.51247
973.15	-0.00012	0.490051
978.15	-0.00012	0.467901
983.15	-0.00013	0.446005
988.15	-0.00013	0.424359
993.15	-0.00014	0.402962
998.15	-0.00014	0.381807
1003.15	-0.00015	0.3609
1008.15	-0.00015	0.340222
1013.15	-0.00016	0.319784
1018.15	-0.00016	0.299571
1023.15	-0.00017	0.279592
1028.15	-0.00017	0.25983
1033.15	-0.00018	0.240284
1038.15	-0.00018	0.220957
1043.15	-0.00019	0.201846
1048.15	-0.00019	0.182938
1053.15	-0.0002	0.164242
1058.15	-0.0002	0.145744
1063.15	-0.0002	0.127452
1068.15	-0.00021	0.109357
1073.15	-0.00021	0.091448

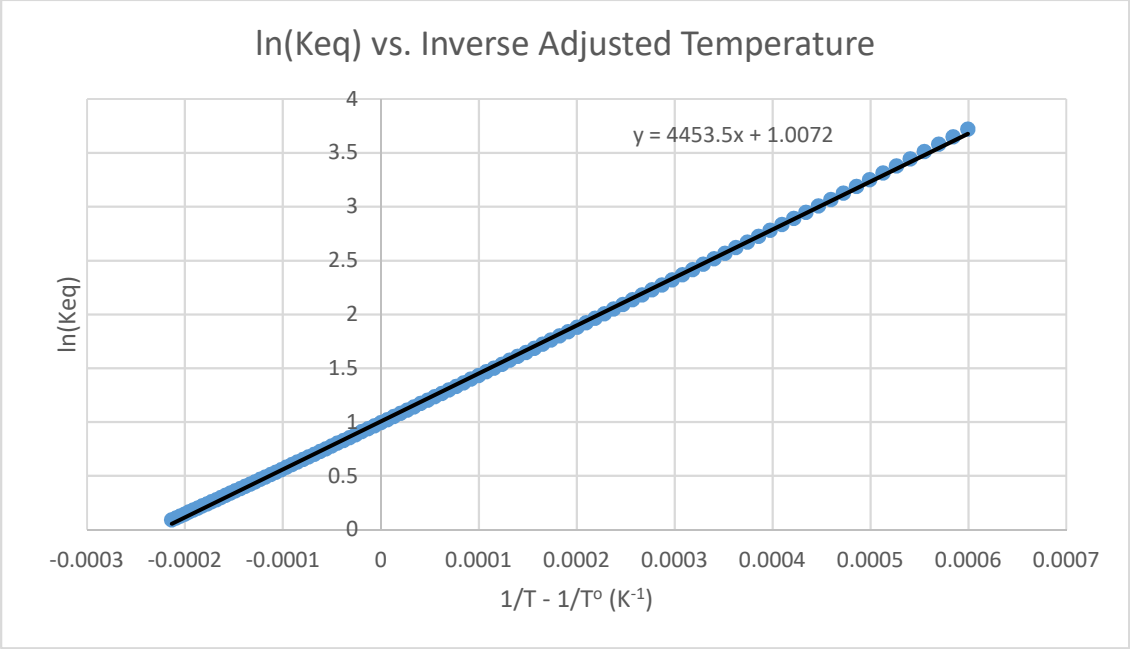

APPENDIX C: GAS MIXTURE SPECIFICATIONS

Scott™ Mini-Mix™ (**23442**) (Analysis by moles)	
Volume (L)	14
Pressure (psig)	240 (@ 21˚C)
Hazards	Contents under pressure, Asphyxiating, Nerve Damage
Carbon Monoxide	7%
Carbon Dioxide	15%
Oxygen	5%
Nitrogen	Balance

Scotty® Analyzed Gases (**23438**) (Analysis by moles)	
Volume (L)	14
Pressure (psig)	240 (@ 21˚C)
Hazards	Contents under pressure, Asphyxiating, Nerve Damage
Carbon Monoxide	0.5%
Carbon Dioxide	0.5%
Oxygen	0.5%
Hydrogen	0.5%
Nitrogen	Balance

MICRO MAT 14 (**GMT10406**) (Analysis by moles)	
Volume (L)	14
Pressure (psig)	240 (@ 21˚C)
Hazards	Contents under pressure, Asphyxiating, Nerve Damage
Carbon Monoxide	7%
Carbon Dioxide	15%
Oxygen	5%
Methane	4.5%
Nitrogen	Balance

MICRO MAT 14 (**GMT10404**) (Analysis by moles)	
Volume (L)	14
Pressure (psig)	240 (@ 21˚C)
Hazards	Contents under pressure, Asphyxiating, Nerve Damage
Carbon Monoxide	5%
Carbon Dioxide	5%
Oxygen	4%
Methane	4%
Hydrogen	4%

Nitrogen	5%
Helium	Balance

MICRO MAT 14 (**GMT10428**) (Analysis by moles)	
Volume (L)	14
Pressure (psig)	240 (@ 21˚C)
Hazards	Contents under pressure, Asphyxiating, Nerve Damage
Carbon Monoxide	0.5%
Carbon Dioxide	0.5%
Oxygen	0.5%
Hydrogen	5%
Nitrogen	Balance

APPENDIX D: GC CALIBRATION CURVES

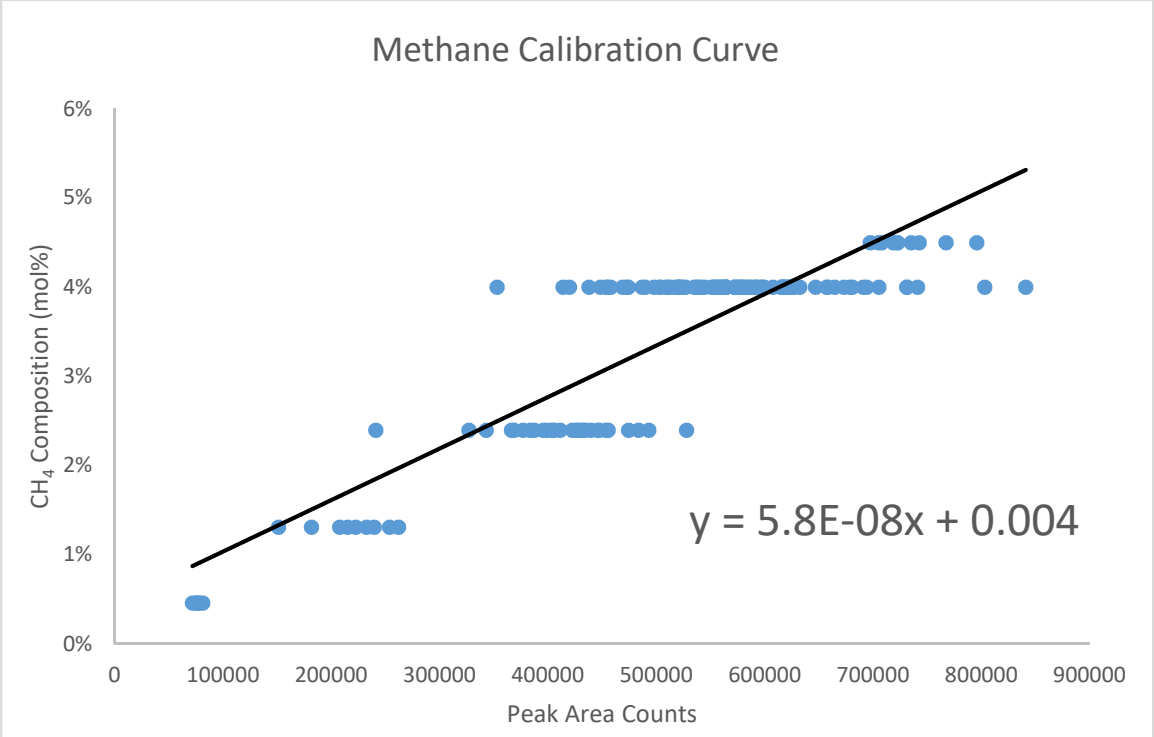

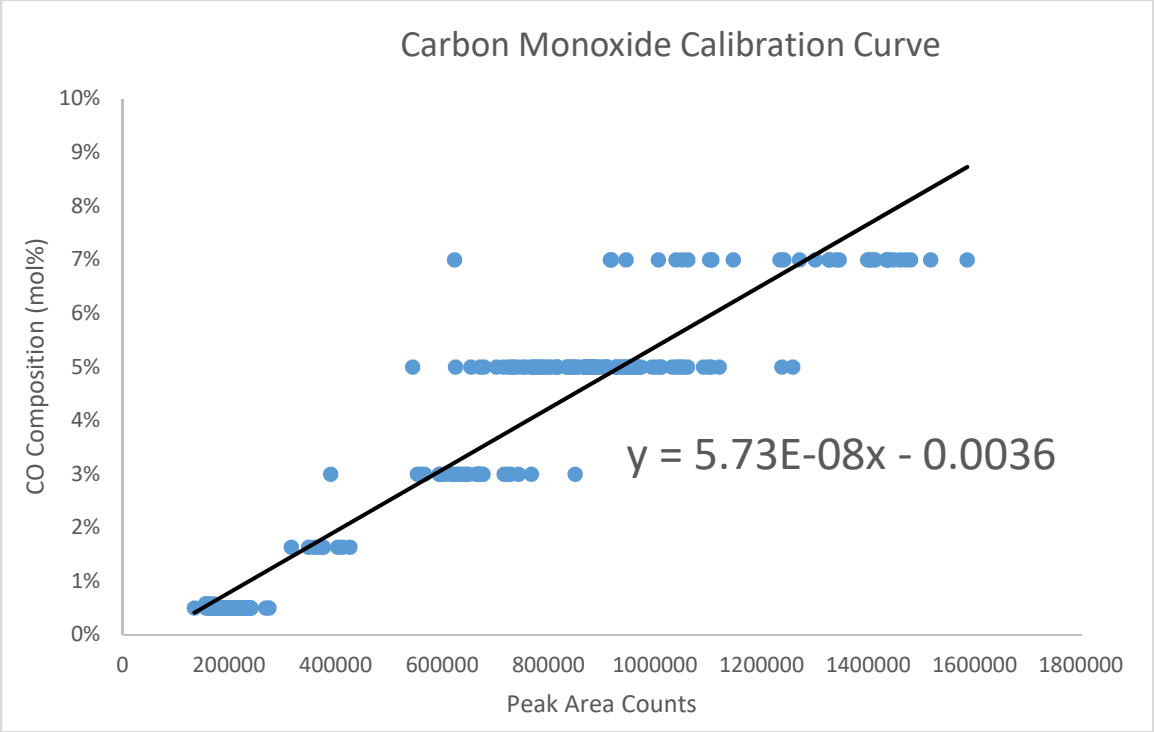

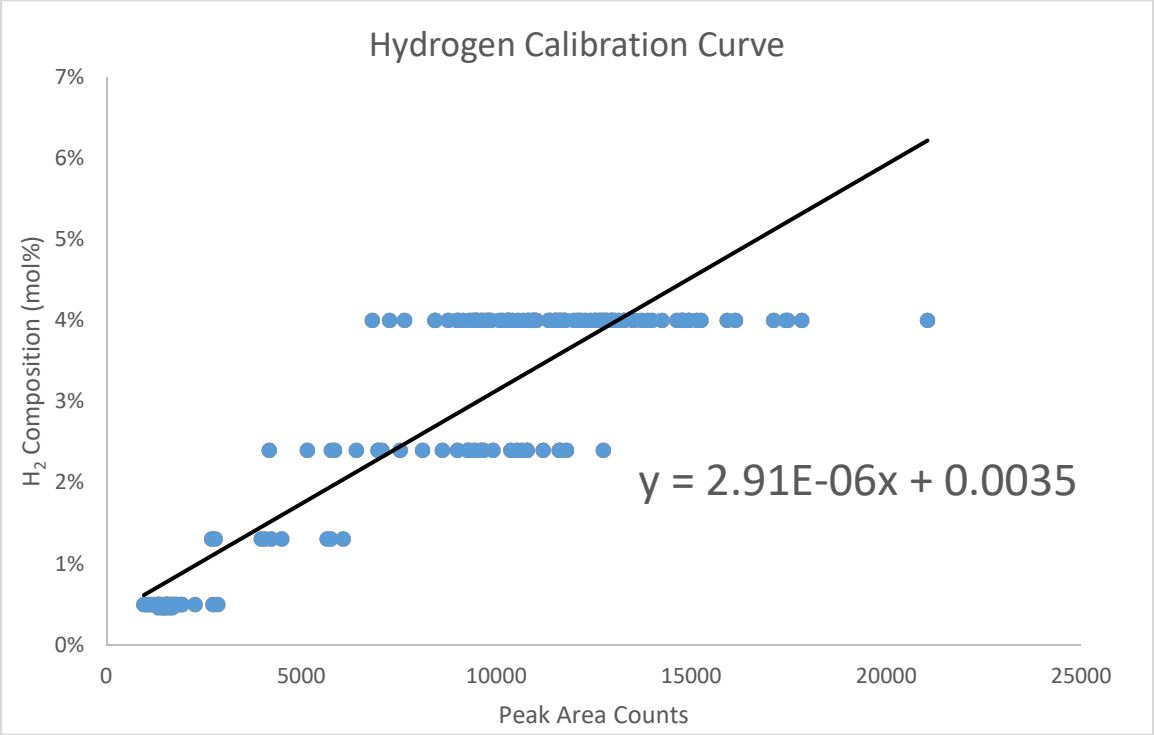
Hydrogen Calibration Curve
7%
6%
5%
4%
3%
2%
1%
0%
H2 Composition (mol%)
0
5000
10000
15000
20000
25000
Peak Area Counts
y = 2.91E-06x + 0.0035

APPENDIX E: DETAILED EXPERIMENTAL PROCEDURE

Sample Cylinder Preparation

- Sample cylinder should be evacuated of previous standard/sample.
- Unscrew one end of the cylinder to open it.
- Discard silica gel and reload with approximately 5 grams of unsaturated silica gel.
- Wrap threads of sample arm in Teflon and reattach to close cylinder.
- Evacuate atmosphere from cylinder and load with approximately 20 psig of a calibration standard mixture with a high concentration of carbon monoxide.
- Allow gas to saturate silica gel for at least 8 hours.
- When reaction is complete, evacuate calibration standard mixture and rinse with approximately 20 psig of He. Then load cylinder with He to atmospheric pressure. This can be done by filling to above atmospheric pressure and then releasing the valve to release excess pressure.
- The sample cylinder is ready for collection of syngas.

Detailed Reaction and Sampling Procedure

- Weigh out the desired substrate amount according to calculations.
- Weigh out the desired amount of catalyst/support powder.
- Measure 20 mL of distilled water. This volume ensures that the water level is above the stirrer blades
- Add these ingredients to the batch reactor.
- Make sure gasket for reactor top is in acceptable condition, otherwise replace.
- Attach reactor top to vessel half and secure the six head bolts tightening in diametrically opposed patterns.

- Place reactor on mixing stand and connect magnetic stirrer to mixing apparatus. Connect the thermocouples and pressure sensor cord to the controller.
- Connect air tank to reactor vessel and load with air to the appropriate pressure according to stoichiometry of polymer oxidation.
- Disconnect air tank and move heating jacket over reactor vessel. Cover the exposed portion of the batch reactor with glass wool insulation without inhibiting the magnetic drive stirrer.
- Connect the cooling jacket to the cold water supply and slowly open the valve.
- Using the controller, set the reaction temperature to 50 degrees above the approximate melting point of the substrate and turn on the heater and stirrer.
- Once the reactor reaches temperature, set to 220°C, 250°C, 275°C, then to the reaction temperature of interest.
- Once the reaction temperature is reached, record the time, pressure, and temperature and allow the reaction to run for the reaction time of interest.

Reactor Cooling, Sampling, and Dismantling

- Upon completion, record the time, pressure and temperature of the reactor and remove the heating jacket from the vessel along with the glass wool. Then submerge the vessel in a 1 L beaker filled with cold water.
- Allow the reactor to cool to approximately 100 °C and replenish the beaker with fresh cooling water.
- Make sure that vessel pressure does not fall below the pressure at the loading phase. This would indicate a sever leak that could compromise results.

- Once reactor temperature is approximately 50 °C and steady, shut off stirrer and connect sample cylinder to sampling arm. Open reactor valve and sample cylinder valve then carefully use sample arm outlet valve to control the pressure release from the reactor. Gather approximately 25 psig of product syngas.
- Allow sample cylinder to cool. Once gauge pressure stops falling, the syngas in ready for injection.
- Before dismantling the reactor, connect the house vacuum system to the reactor sampling arm and carefully bring the reactor pressure down to 25 psia.
- Reactor can then be detached from controller and mixing apparatus and disassembled.
- Cold water flow through the cooling jack can be stopped when the reactor temperature is 30 °C or lower.
- Once the top of the reactor is off, use a pipette and a laboratory spatula to gather as much of the solid residual as possible. A good portion may be stuck to the stirrer. 10 mL of distilled water should be used to rinse the reactor vessel and the rinsate should be gathered and added to the gathered solid residual.
- Use water and cotton tip applicators to scrub the walls and bottom of the reactor vessel until there is no black residue.

Gas Chromatography Injection Procedure

- Once the sample cylinder is loaded, time should be allowed for the vessel to cool and for the pressure to reach its room temperature reading. This pressure is then recorded as it is crucial to the analysis when accounting for the dilution of He in the cylinder.
- Change liner wool plug. It should be approx. 10 mm long and 35 mm from inlet.

- Open the appropriate GC Run Method. Allow the flow rates to reach set point values and turn on the detector.
- Adjust the signal to zero and prepare the software for data collection by selecting "Start Single Run"
- Use the syringe and manipulate the sampling valve to extract 1 mL of gas from the sample cylinder.
- Insert the syringe needle into the injection port as straight as possible and immediately push the plunger down while simultaneously hitting the "Start" button on the GC.
- Hold the syringe in the injection port for exactly 5 seconds and then remove quickly. The analysis has begun.

Detailed Differential Scanning Calorimetry (DSC) Procedure

- If centrifuge tube has not had time to allow solid residual to settle and separate from the water phase, centrifuge the sample.
- Remove and discard the water phase until little is left but the solid phase.
- Use a laboratory spatula to load a large amount of wet solid onto an aluminum pan. If this proves difficult, one can add a few drops of distilled water and transfer the solid/liquid mixture to a pan via pipette.
- To dry the sample, begin by taring an aluminum pan in the Thermal Gravimetric Analyzer (TGA).
- Open the N_2 tank to provide purge flow to the TGA
- Load the pan onto the TGA sampling arm and use the instrument controls to load the pan into the furnace.

- Run the TGA program for drying at 120°C and record the weight of the dried sample once the run has completed.
- Transfer the sample and the pan to the DSC and place it on the crucible next to the reference pan.
- Close the lid to the DSC and run the program. Run the program two more times. This allows for the melting in the first run to evenly distribute the material in the aluminum pan so that results in the second and third trials are more accurate.
- Peaks in the Thermal Analysis DSC software are then manually integrated for quantitative analysis.

Safety Precautions

- Wear heat resistant gloves when handling the reactor heating jacket at the end of a reaction.
- Do not attempt to handle the reactor until the temperature readings are at least below 40 °C.
- Use the lab hood screen to protect against boiling water and steam from the cooling water beaker.
- Wear latex gloves when handling glass wool.

APPENDIX F: DETERMINATION OF UNCERTAINTY

Percent Gasification Uncertainty

$$\frac{dX_A}{dP^{col}} = \frac{\frac{V_2}{R * T^{col}} * \left(y_{CO} + y_{CO_2} + y_{CH_4}\right)}{\frac{m_A}{M_A} * c}$$

$$\frac{dX_A}{dT^{col}} = \frac{-\frac{P^{col} * V_2}{R * (T^{col})^2} * \left(y_{CO} + y_{CO_2} + y_{CH_4}\right)}{\frac{m_A}{M_A} * c}$$

$$\frac{dX_A}{dy_{CO}} = \frac{\frac{P^{col} * V_2}{R * T^{col}} * y_{CO}}{\frac{m_A}{M_A} * c}$$

$$\frac{dX_A}{dy_{CO_2}} = \frac{\frac{P^{col} * V_2}{R * T^{col}} * y_{CO_2}}{\frac{m_A}{M_A} * c}$$

$$\frac{dX_A}{dy_{CH_4}} = \frac{\frac{P^{col} * V_2}{R * T^{col}} * y_{CH_4}}{\frac{m_A}{M_A} * c}$$

$$\frac{dX_A}{dm_A} = \frac{\frac{P^{col} * V_2}{R * T^{col}} * \left(y_{CO} + y_{CO_2} + y_{CH_4}\right)}{-\frac{(m_A)^2}{M_A} * c}$$

$$\frac{dX_A}{dV_2} = \frac{\frac{P^{col}}{R * T^{col}} * \left(y_{CO} + y_{CO_2} + y_{CH_4}\right)}{\frac{m_A}{M_A} * c}$$

Molar Composition Uncertainties

$$\frac{dy_i}{dm_i} = \frac{P^{He} + P^{sam}}{P^{sam}} * x_i$$

$$\frac{dy_i}{dx_i} = \frac{P^{He} + P^{sam}}{P^{sam}} * m_i$$

$$\frac{dy_i}{dP^{sam}} = \frac{-(m_i * x_i * P^{He}) - (b_i * P^{He})}{(P^{sam})^2}$$

$$\frac{dy_i}{db_i} = \frac{P^{He} + P^{sam}}{P^{sam}}$$

$$\omega_{x_i} = \frac{\sigma_i}{\sqrt{n}}$$

$$\omega_{n_i} = \sqrt{\left(\frac{dn_i}{dP^{col}} * \omega_{P^{col}}\right)^2 + \left(\frac{dn_i}{dT^{col}} * \omega_{T^{col}}\right)^2 + \left(\frac{dn_i}{dV_2} * \omega_{V_2}\right)^2 + \left(\frac{dn_i}{dy_i} * \omega_{y_i}\right)^2}$$

$$\frac{dn_i}{dP^{col}} = \frac{V_2}{R * T^{col}} * y_i$$

$$\frac{dn_i}{dT^{col}} = -\frac{P^{col} * V_2}{R * (T^{col})^2} * y_i$$

$$\frac{dn_i}{dV_2} = \frac{P^{col} * V_2}{R * T^{col}} * y_i$$

$$\frac{dn_i}{dy_i} = \frac{P^{col} * V_2}{R * T^{col}}$$

$$\omega_{N_A^o} = \sqrt{\left(\frac{1}{M_A} * \omega_{m_A}\right)^2}$$